Supporting Information

Solvent modulation of the morphology of homochiral gadolinium coordination polymers and its impact on circularly polarized luminescence

Ting Hou,[a] Chen-Chen Zhao,[b] Song-Song Bao,[a] Zhi-Min Zhai,[a] and Li-Min Zheng[a,*]

[a] T. Hou, Prof. Dr. S.-S. Bao, Z.-M. Zhai, and Prof. Dr. L.-M. Zheng
State Key Laboratory of Coordination Chemistry, School of Chemistry and Chemical Engineering, Nanjing University, Nanjing, 210023, P. R. China
E-mail: lmzheng@nju.edu.cn

[b] C.-C. Zhao
Theoretical and Computational Chemistry Institute, School of Chemistry and Chemical Engineering, Nanjing University, Nanjing 210023, P. R. China.

*Correspondence: lmzheng@nju.edu.cn

Content

I. Experimental section

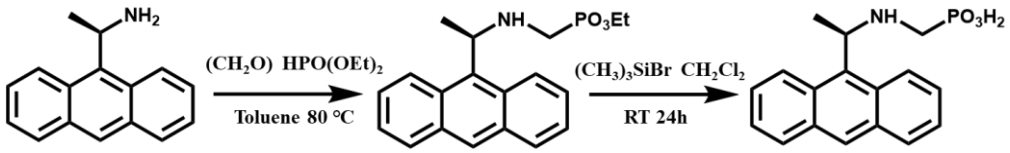

Scheme S1. Synthetic routes of *R*-AnempEt$_2$ and *R*-AnempH$_2$ ligands.

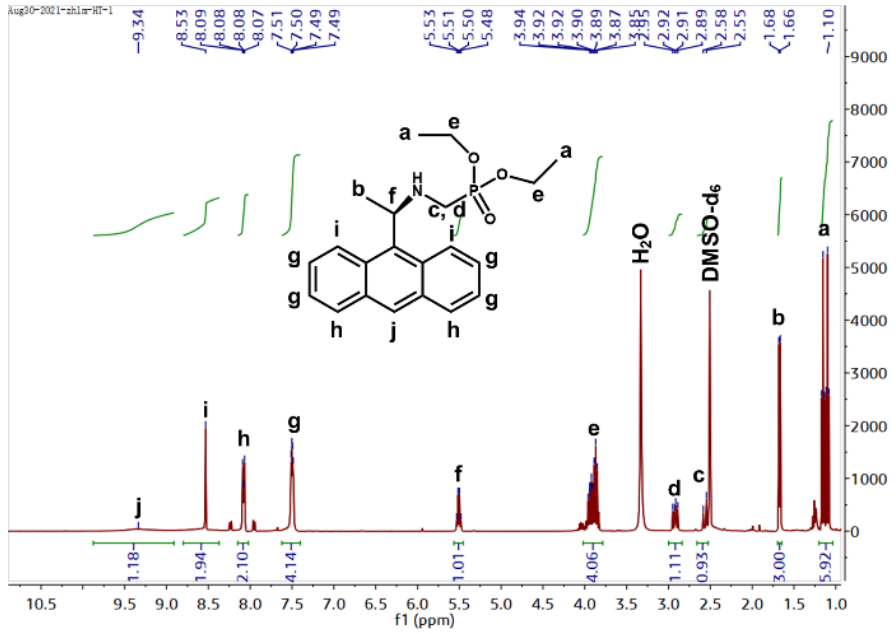

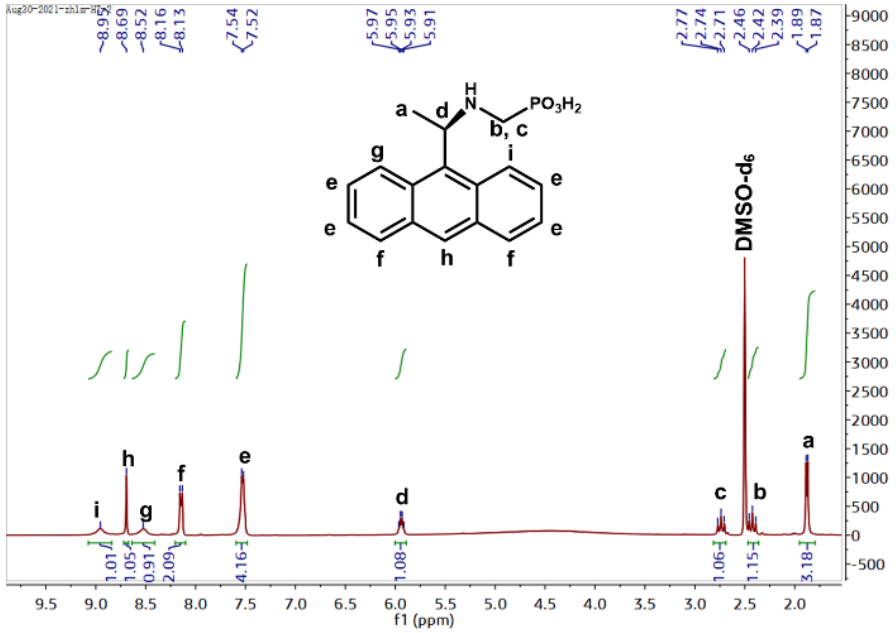

Figure S1. ^{1}H NMR spectra of *R*-AnempEt$_2$ and *R*-AnempH$_2$ ligand (400 MHz, DMSO-d$_6$).

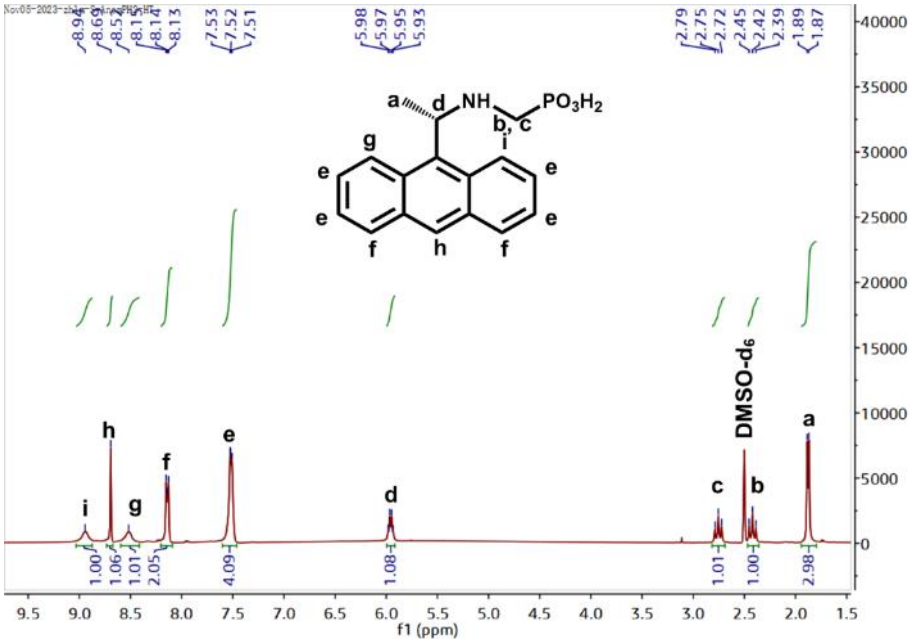

Figure S2. ^{1}H NMR spectra of *S*-AnempH_2 ligand (400 MHz, DMSO-d_6).

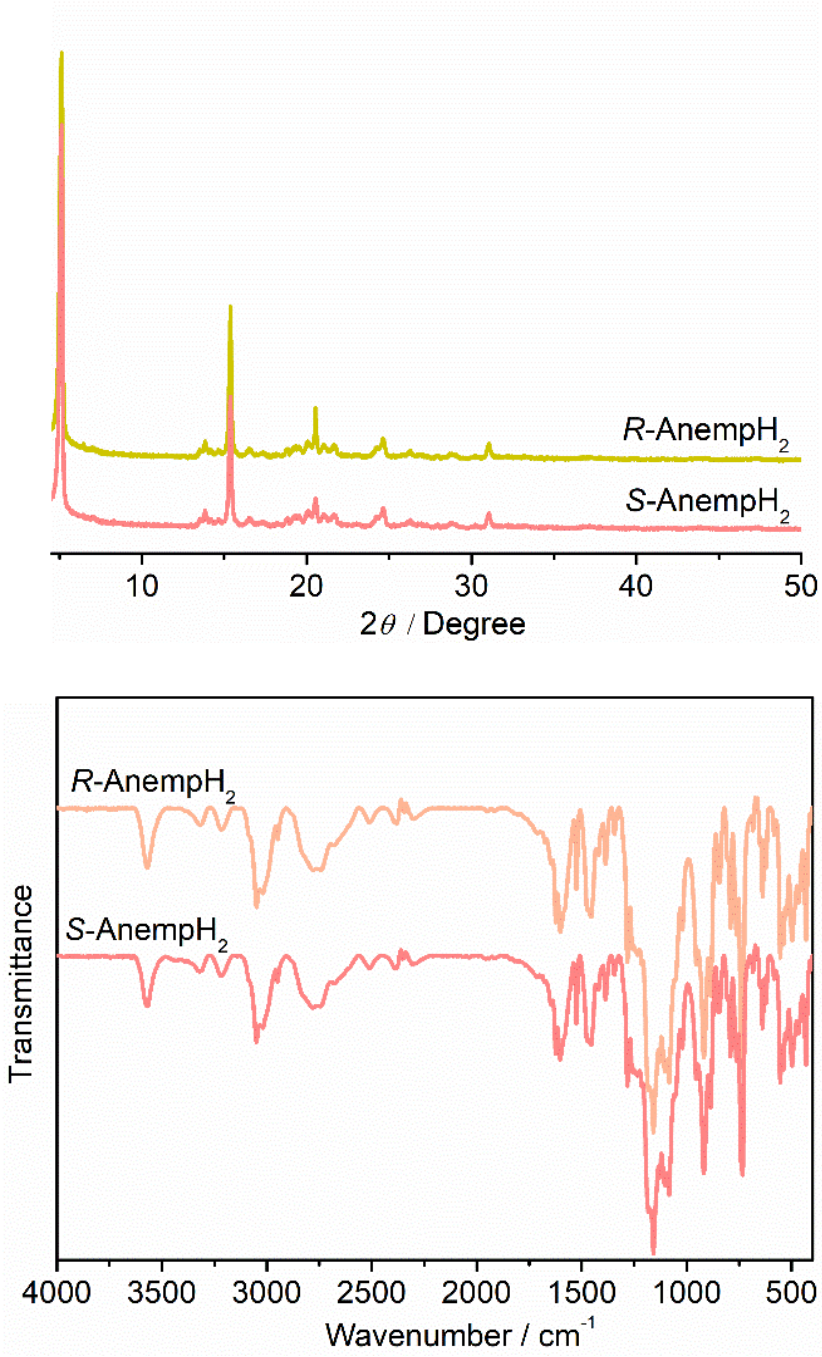

Figure S3. (top) PXRD and (bottom) IR spectra of *R*-AnempH$_2$ and *S*-AnempH$_2$ ligands.

II. Synthesis and characterization of chiral spiral bundles, crystals and spindle-shaped particles of $Gd(NO_3)_3$/*R*-,*S*-AnempH_2 assemblies

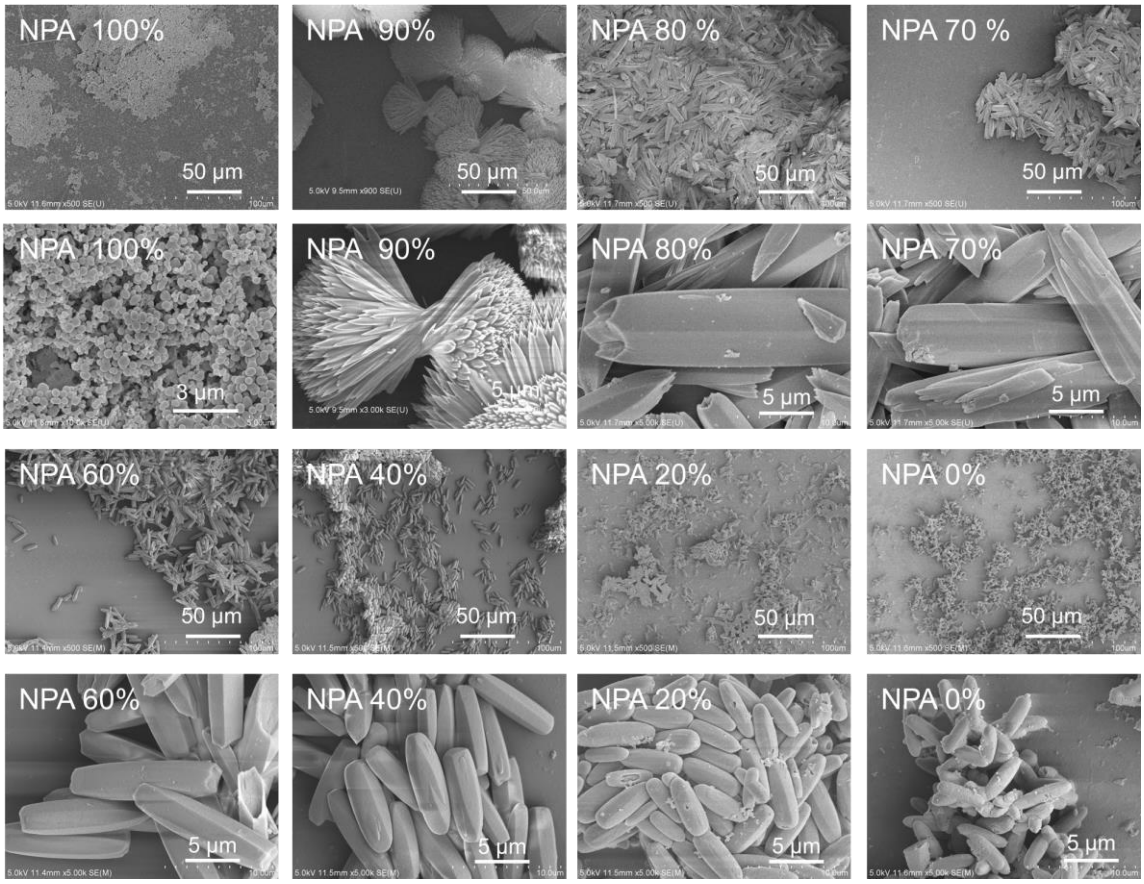

Figure S4. SEM images showing the morphology of reaction products of Gd^{3+}/*R*-AnempH_2 (1:3) obtained in different volume ratio of NPA/DMF (total volume 5 mL) and 0.5 mL H_2O at 100°C.

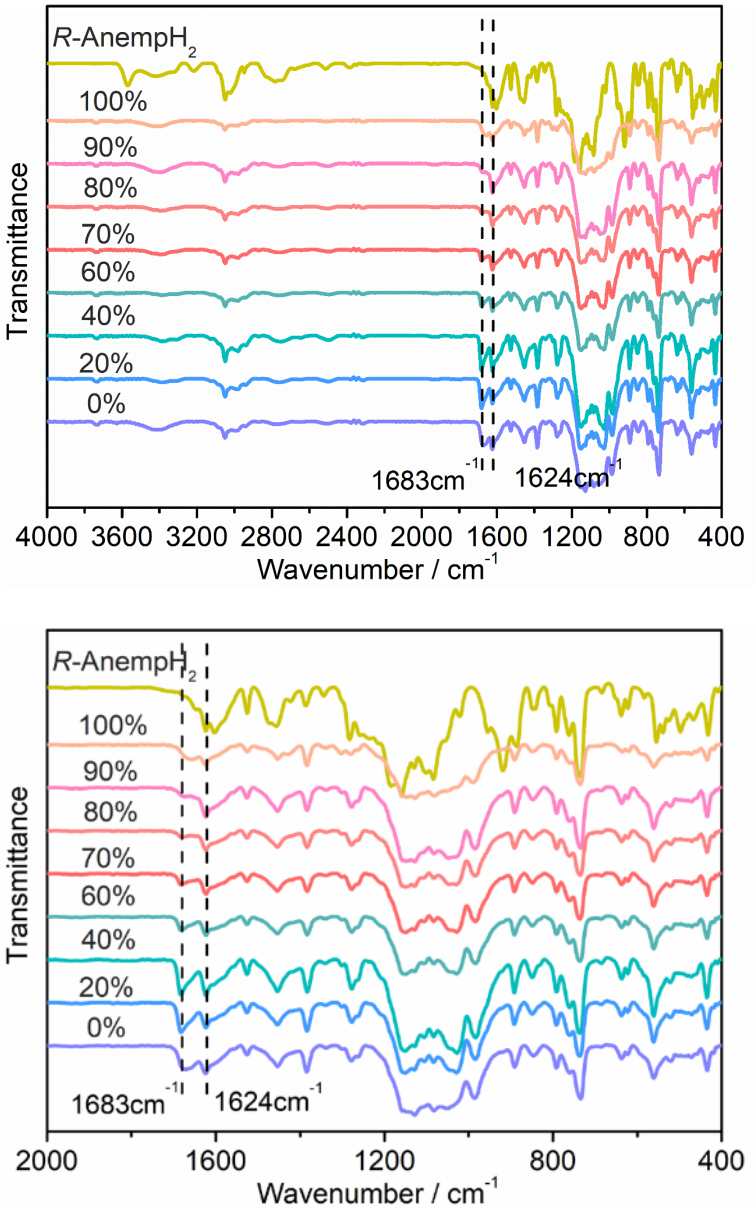

Figure S5. IR spectra of the reaction products of Gd^{3+}/*R*-AnempH_2 (1:3) obtained in different volume ratio of NPA/DMF (total volume 5 mL) and 0.5 mL H_2O at 100°C (up: 4000-400 cm^{-1}, bottom: 2000-400 cm^{-1}).

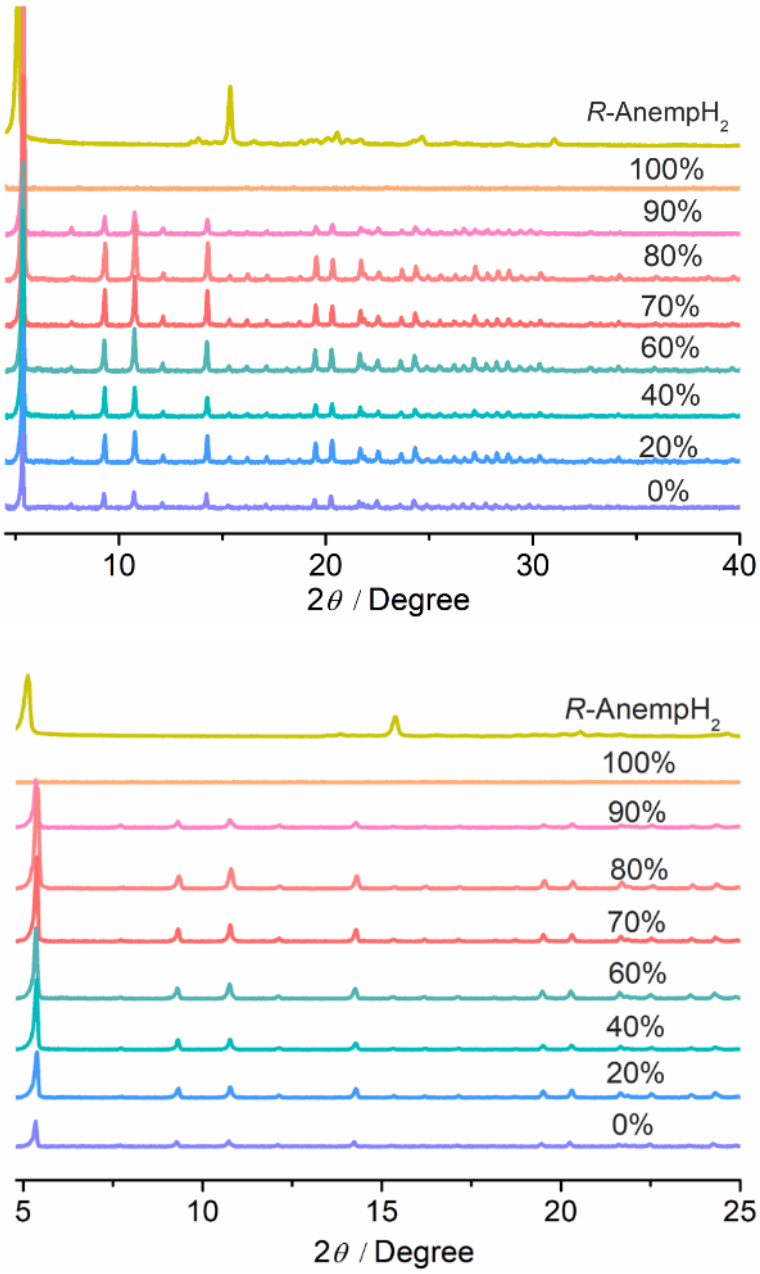

Figure S6. PXRD patterns of the reaction products of Gd^{3+}/*R*-AnempH_2 (1:3) obtained in different volume ratio of NPA/DMF (total volume 5 mL) and 0.5 mL H_2O at 100°C (up: 2θ 4.5-40°, bottom: 2θ 4。5-25°).

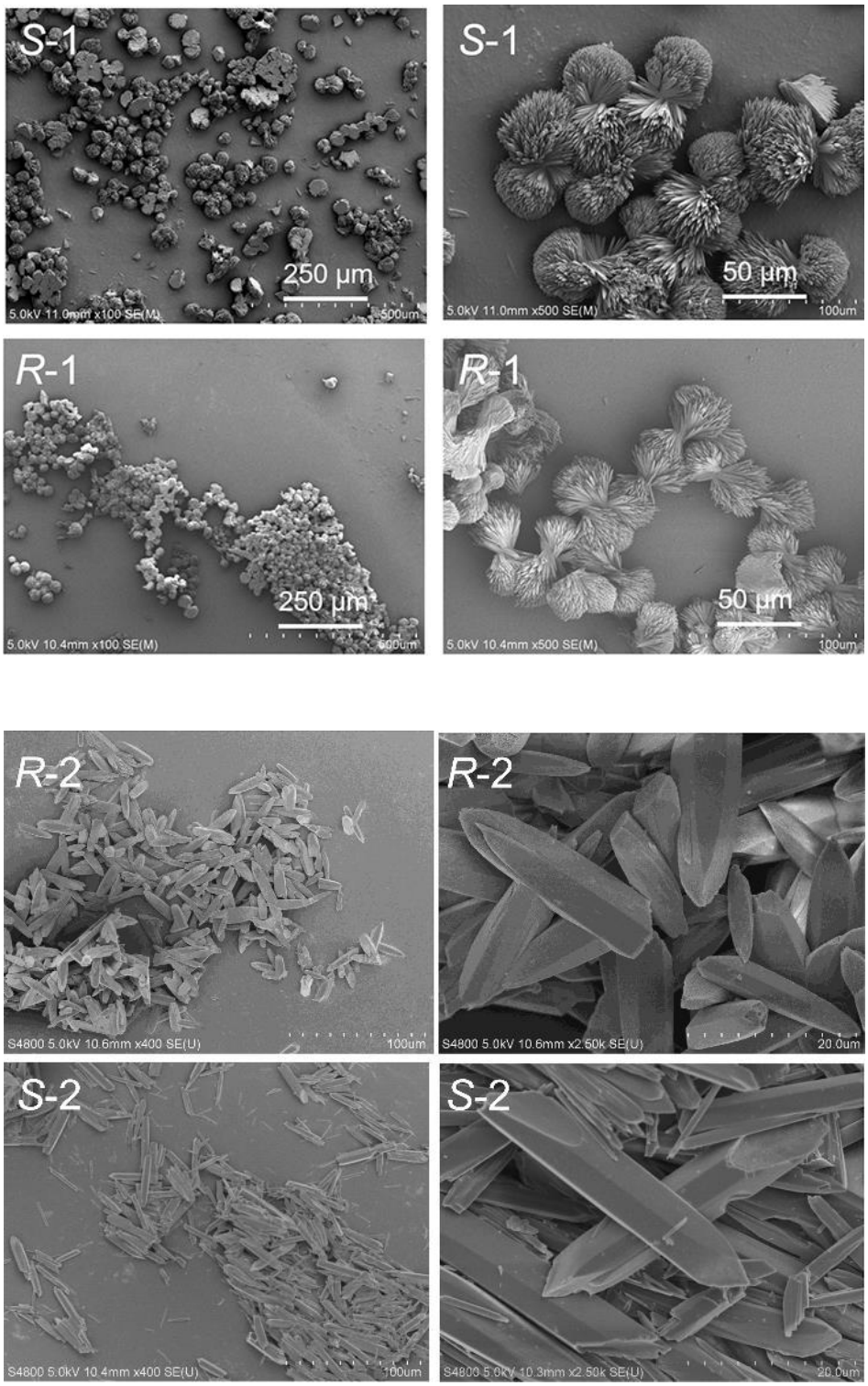

Figure S7. SEM images of *R*/*S*-**1** and *R*/*S*-**2**.

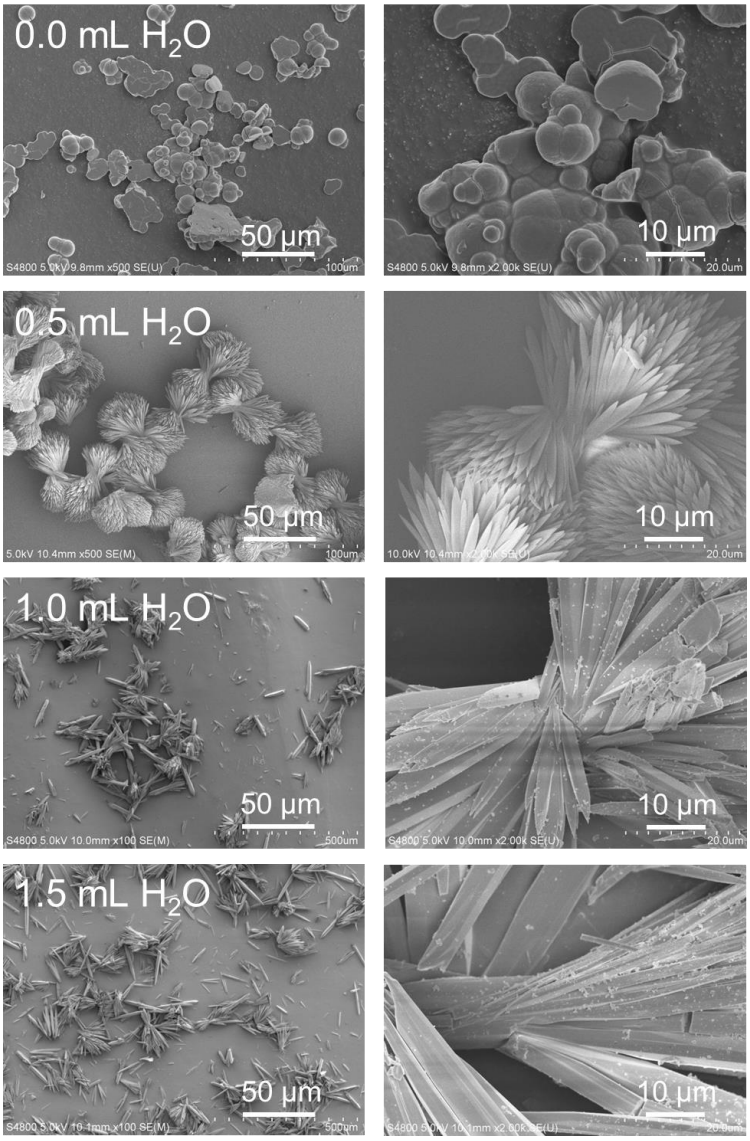

Figure S8. SEM images showing the morphology of the reaction products of Gd^{3+}/*R*-AnempH_2 (1:3) obtained in 90 vol % NPA/DMF (total volume 5 mL) and different volume of deionized water (0.0, 0.5, 1.0 1.5 mL) at 100°C.

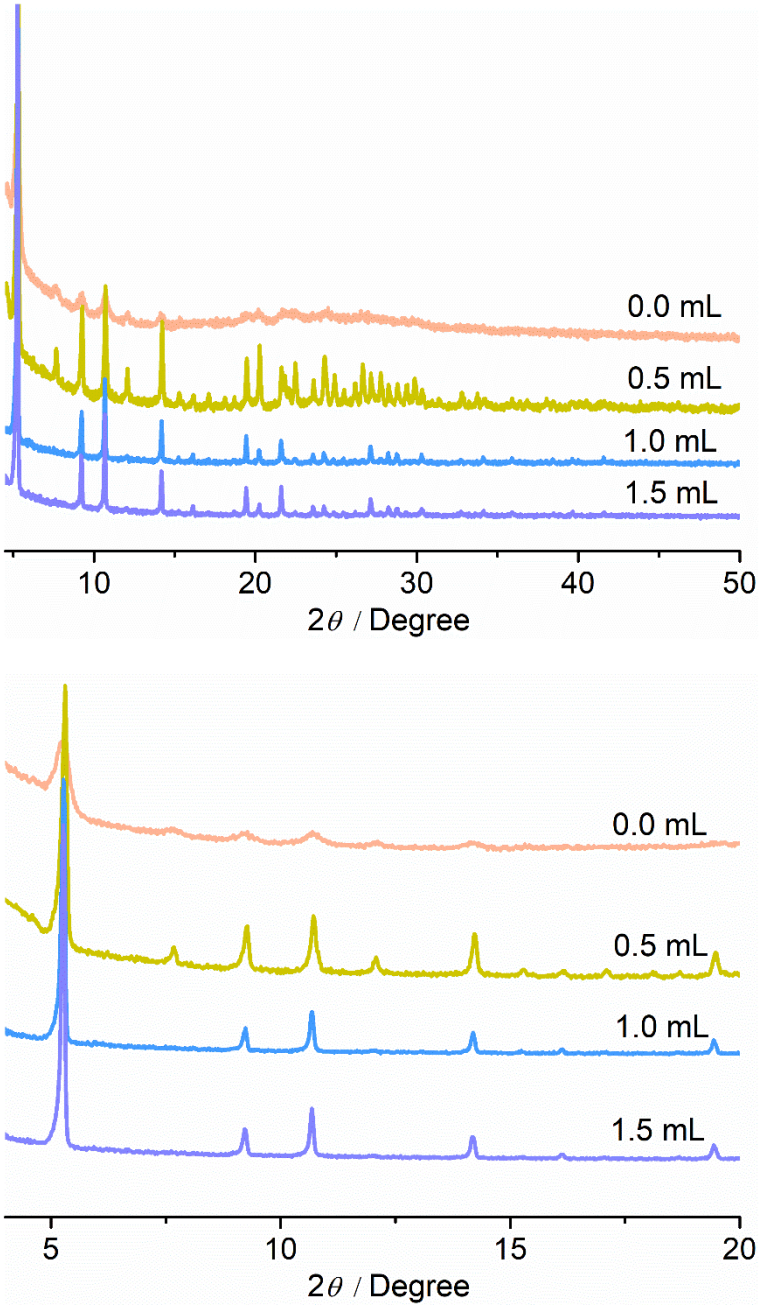

Figure S9. PXRD patterns of the reaction products of Gd^{3+}/*R*-AnempH_2 (1:3) obtained in 90 vol % NPA/DMF (total volume 5 mL) and different volume of deionized water (0.0, 0.5, 1.0 1.5 mL) at 100°C (up: 2θ 4-40°, bottom: 2θ 4-20°).

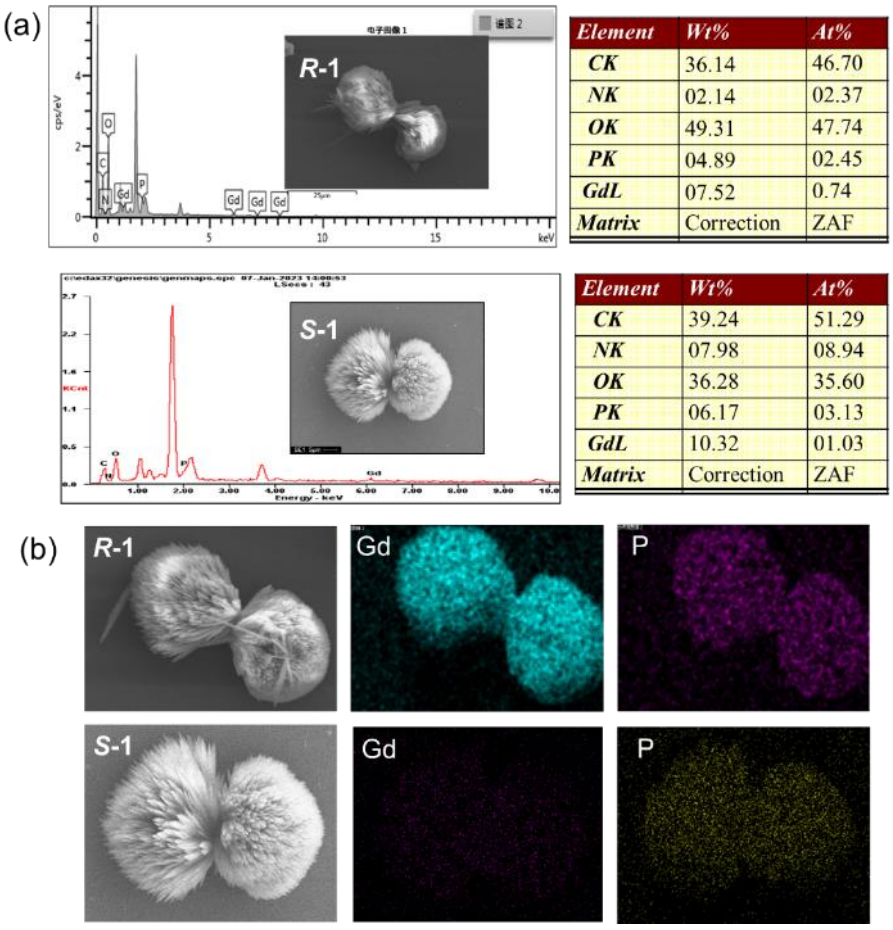

Element	Wt%	At%
CK	36.14	46.70
NK	02.14	02.37
OK	49.31	47.74
PK	04.89	02.45
GdL	07.52	0.74
Matrix	Correction	ZAF

Element	Wt%	At%
CK	39.24	51.29
NK	07.98	08.94
OK	36.28	35.60
PK	06.17	03.13
GdL	10.32	01.03
Matrix	Correction	ZAF

Figure S10. (a) EDS results and (b) mapping images of ***R*-1** and ***S*-1**.

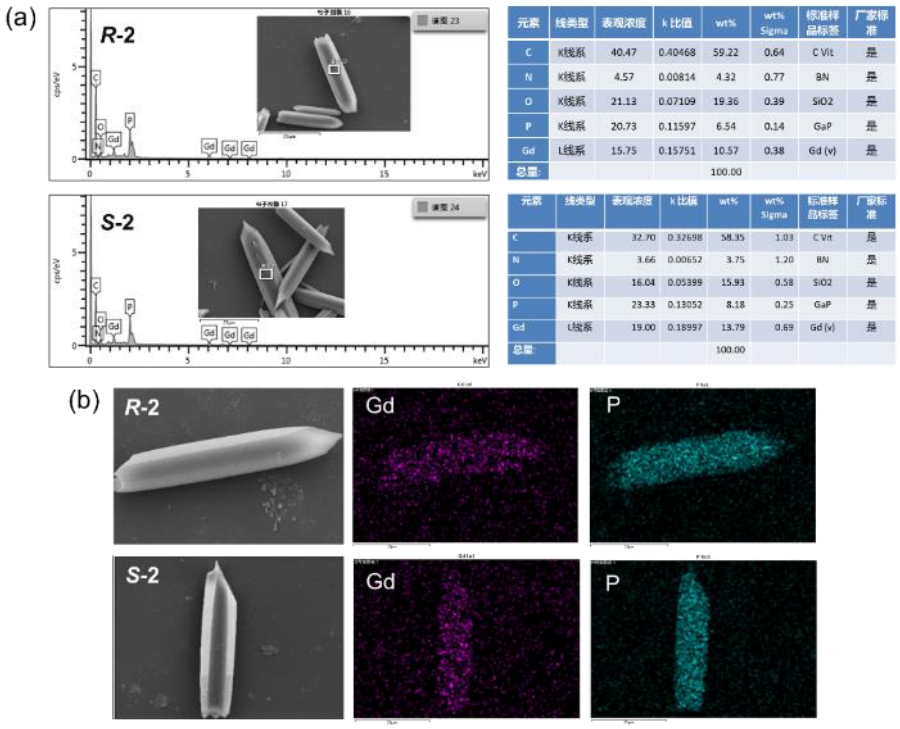

元素	线类型	表观浓度	k 比值	wt%	wt% Sigma	标准样品标签	厂家标准
C	K线系	40.47	0.40468	59.22	0.64	C Vit	是
N	K线系	4.57	0.00814	4.32	0.77	BN	是
O	K线系	21.13	0.07109	19.36	0.39	SiO2	是
P	K线系	20.73	0.11597	6.54	0.14	GaP	是
Gd	L线系	15.75	0.15751	10.57	0.38	Gd (v)	是
总量:				100.00			

元素	线类型	表观浓度	k 比值	wt%	wt% Sigma	标准样品标签	厂家标准
C	K线系	32.70	0.32698	58.35	1.03	C Vit	是
N	K线系	3.66	0.00652	3.75	1.20	BN	是
O	K线系	16.04	0.05399	15.93	0.58	SiO2	是
P	K线系	23.33	0.13052	8.18	0.25	GaP	是
Gd	L线系	19.00	0.18997	13.79	0.69	Gd (v)	是
总量:				100.00			

Figure S11. (a) EDS result and (b) mapping images of ***R*-2** and ***S*-2**.

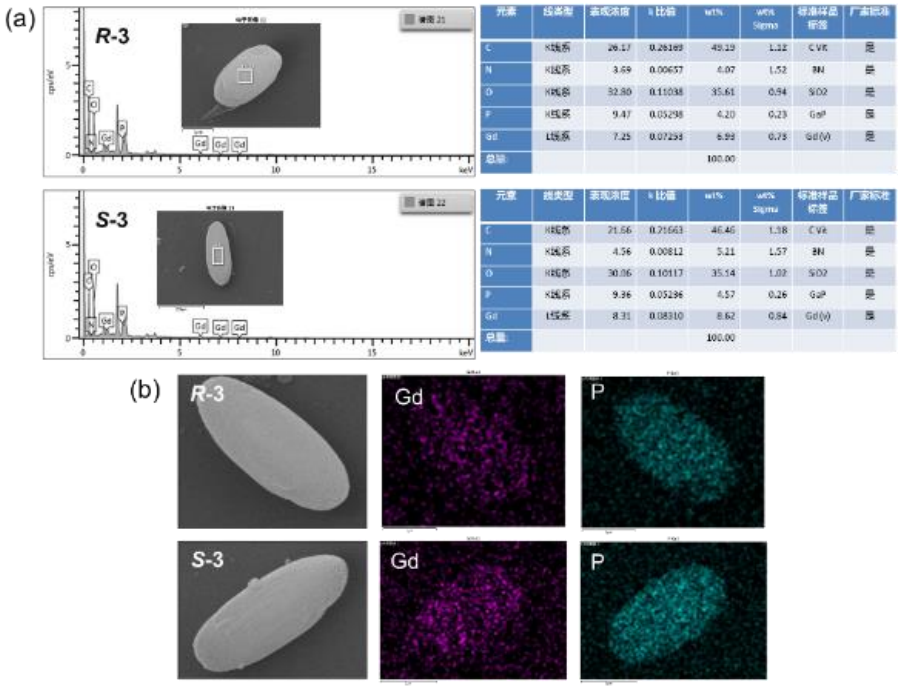

元素	线类型	表观浓度	k 比值	wt%	wt% Sigma	标准样品标签	厂家标准
C	K线系	26.17	0.26169	48.19	1.12	C Vit	是
N	K线系	3.69	0.00657	4.07	1.52	BN	是
O	K线系	32.80	0.11038	35.61	0.94	SiO2	是
P	K线系	9.47	0.05298	4.20	0.23	GaP	是
Gd	L线系	7.25	0.07253	8.93	0.78	Gd (v)	是
总量:				100.00			

元素	线类型	表观浓度	k 比值	wt%	wt% Sigma	标准样品标签	厂家标准
C	K线系	21.66	0.21663	46.46	1.38	C Vit	是
N	K线系	4.56	0.00812	5.21	1.57	BN	是
O	K线系	30.86	0.10117	35.14	1.02	SiO2	是
P	K线系	9.36	0.05236	4.57	0.26	GaP	是
Gd	L线系	8.31	0.08310	8.62	0.84	Gd (v)	是
总量:				100.00			

Figure S12. (a) EDS result and (b) mapping images of ***R*-3**, ***S*-3**.

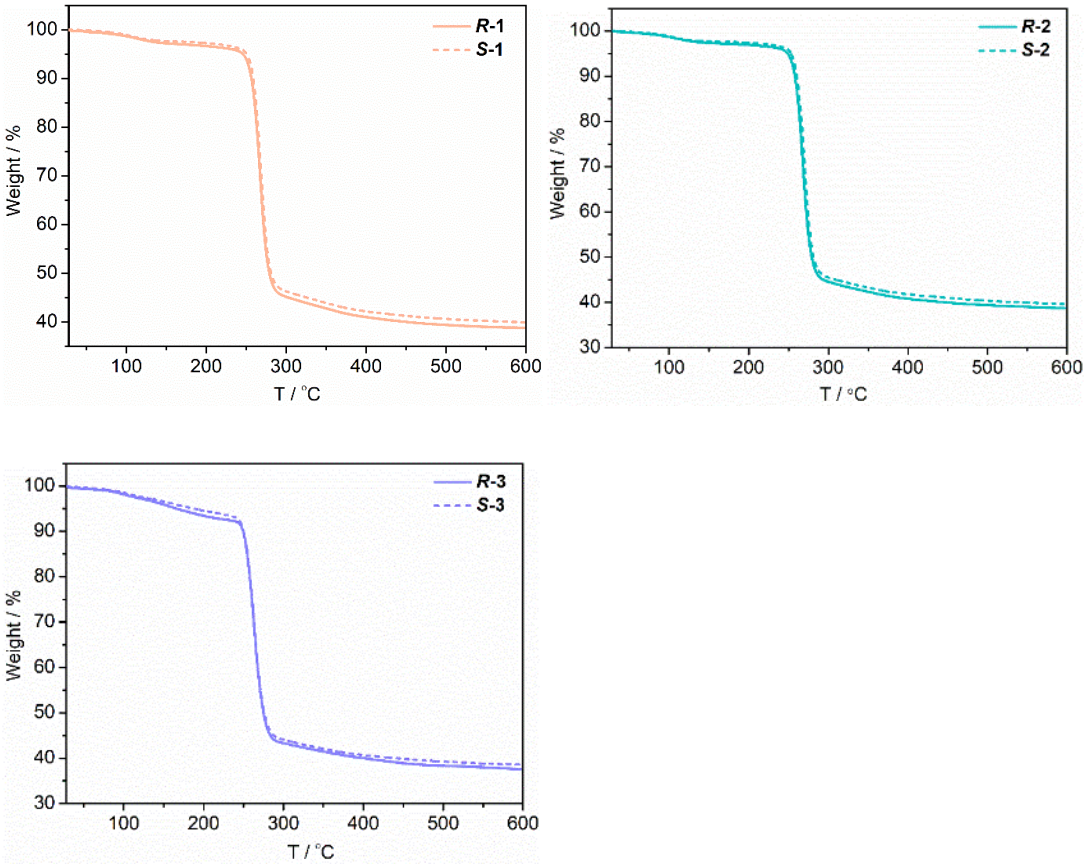

Figure S13. TG curves of ***R-,S*-1**, ***R-,S*-2** and ***R-,S*-3**. The weight losses are 3.3% (for ***R*-1**), 3.1% (for ***S*-1**), 3.0% (***R*-2**) and 2.9% (for ***S*-2**) in the temperature 30-150°C, which agree well with the values expected for the removal of two lattice water molecules (calcd. 3.2%). For ***R*-3** and ***S*-3**, the weight losses are 7.4% and 6.7% in the temperature 30-220°C, which agree well with the values expected for the removal of three lattice water molecules and 0.5 DMF molecules (calcd. 7.2%).

Table S1. Element analysis of ***R*-1**, ***S*-1**, ***R*-2**, ***S*-2**, ***R*-3** and ***S*-3**.

	Chemical formula	Experiment / %	Calculation / %
***R*-1**	Gd(*R*-AnempH)$_3$·2H$_2$O	C 53.69; H 4.99; N 3.77	C 53.87; H 4.84; N 3.70
***S*-1**	Gd(*S*-AnempH)$_3$·2H$_2$O	C 53.94; H 4.91; N 3.72	C 53.87; H 4.84; N 3.70
***R*-2**	Gd(*R*-AnempH)3·2H$_2$O	C 53.71; H 5.11; N 3.80	C 53.87; H 4.84; N 3.70
***S*-2**	Gd(*S*-AnempH)$_3$·2H$_2$O	C 53.95; H 5.04; N 3.77	C 53.87; H 4.84; N 3.70
***R*-3**	Gd(*R*-AnempH)$_3$·3H$_2$O·0.5DMF	C 52.63; H 4.89; N 4.47	C 52.91; H 5.08; N 4.11
***S*-3**	Gd(*S*-AnempH)$_3$·3H$_2$O·0.5DMF	C 52.70; H 5.18; N 4.40	C 52.91; H 5.08; N 4.11

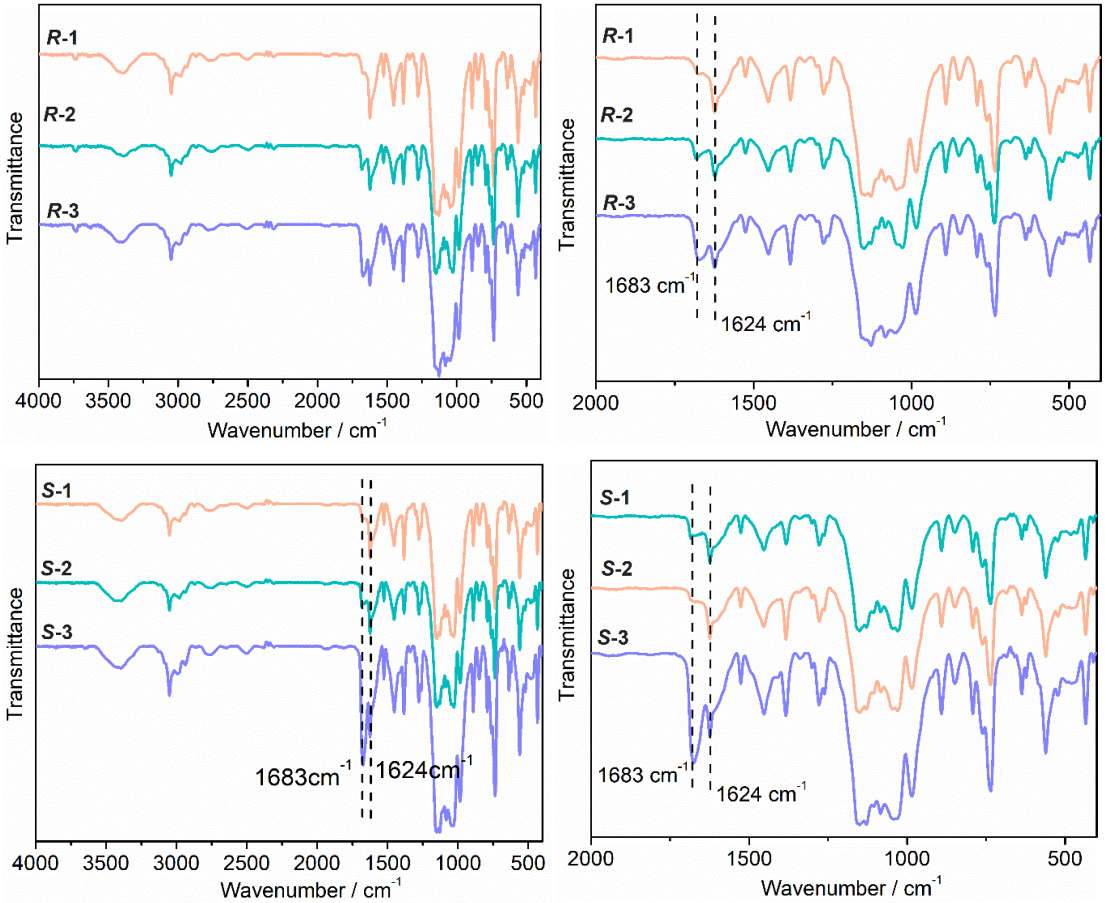

Figure S14. IR spectra of the *R*- and *S*-isomers of **1**, **2** and **3** (left: 4000-400 cm^{-1}, right: 2000-400 cm^{-1}).

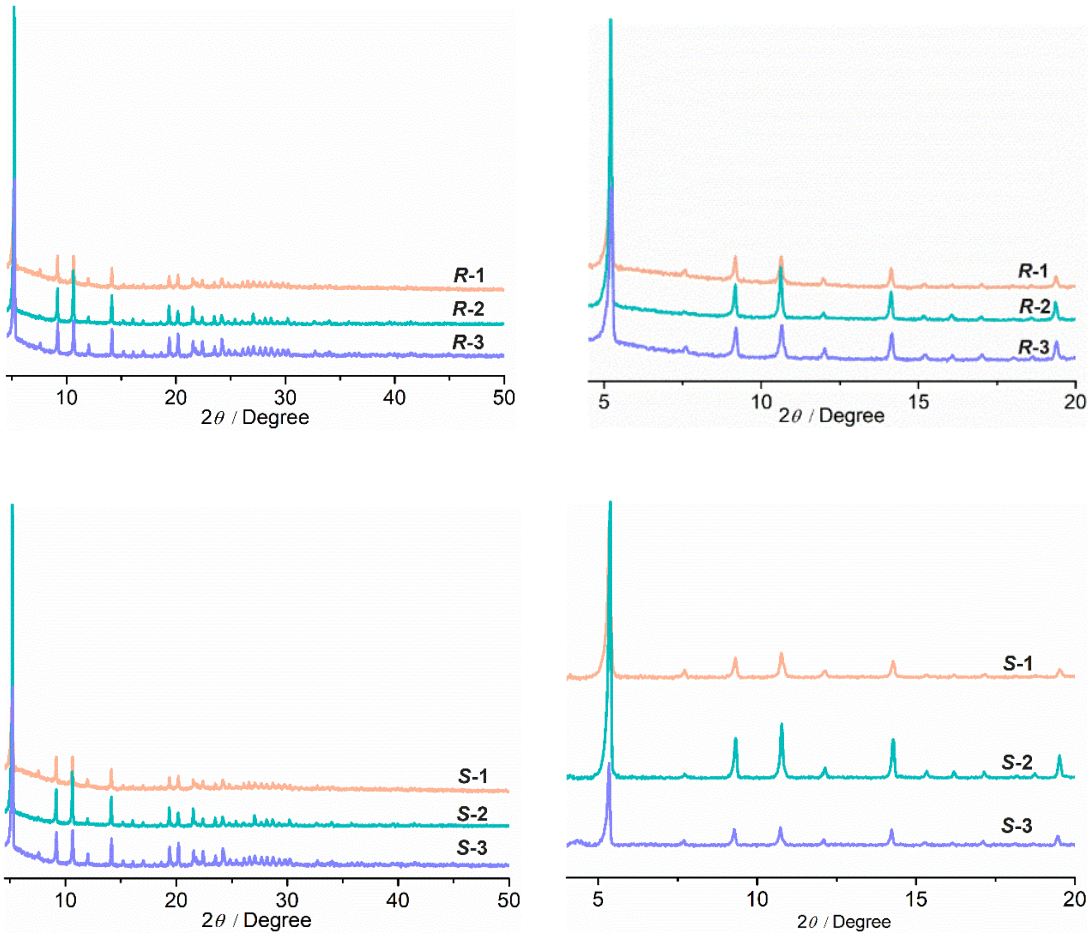

Figure S15. PXRD patterns of the *R*- and *S*-isomers of **1**, **2** and **3** (left: 2θ 4-50°, right: 2θ 4-20°).

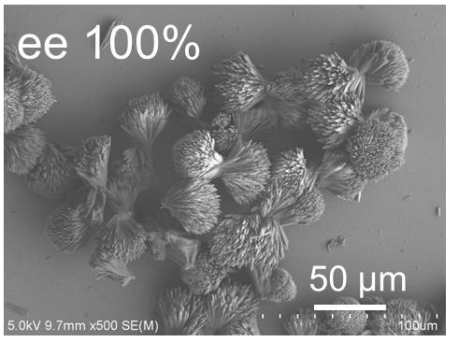
ee 100%
50 µm
5.0kV 9.7mm x500 SE(M)
100um

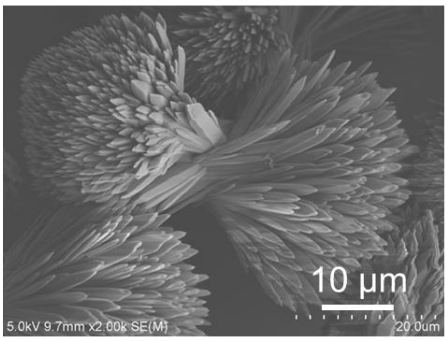
10 µm
5.0kV 9.7mm x2.00k SE(M)
20.0um

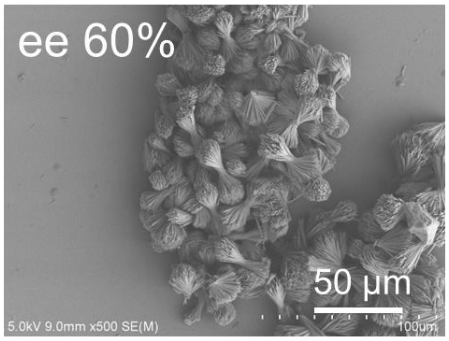
ee 60%
50 µm
5.0kV 9.0mm x500 SE(M)
100um

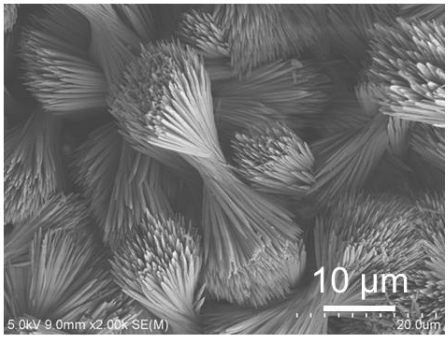
10 µm
5.0kV 9.0mm x2.00k SE(M)
20.0um

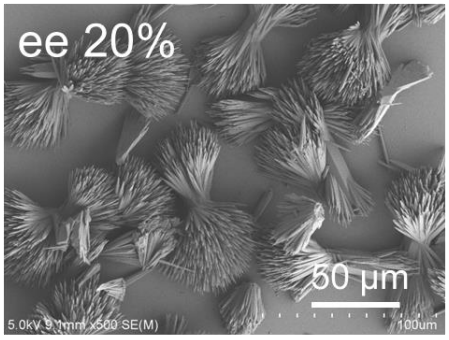
ee 20%
50 µm
5.0kV 9.1mm x500 SE(M)
100um

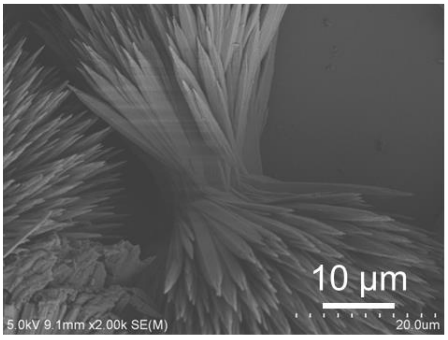
10 µm
5.0kV 9.1mm x2.00k SE(M)
20.0um

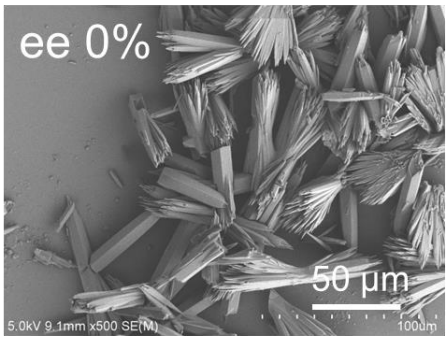
ee 0%
50 µm
5.0kV 9.1mm x500 SE(M)
100um

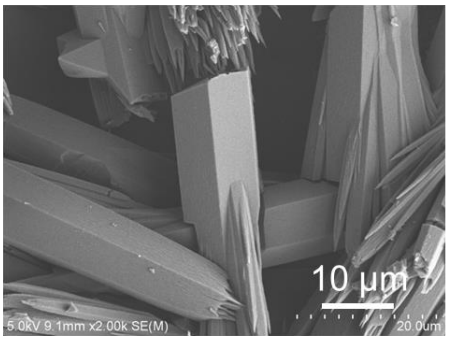
10 µm
5.0kV 9.1mm x2.00k SE(M)
20.0um

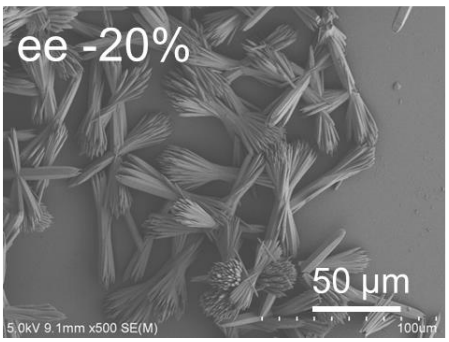
ee -20%
50 µm
5.0kV 9.1mm x500 SE(M)
100um

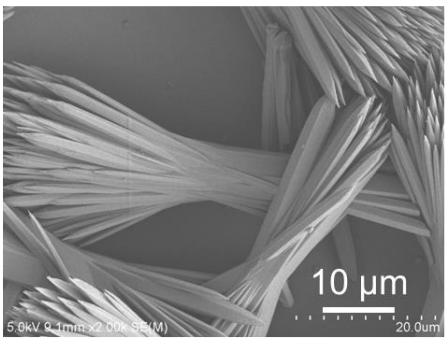
10 µm
5.0kV 9.1mm x2.00k SE(M)
20.0um

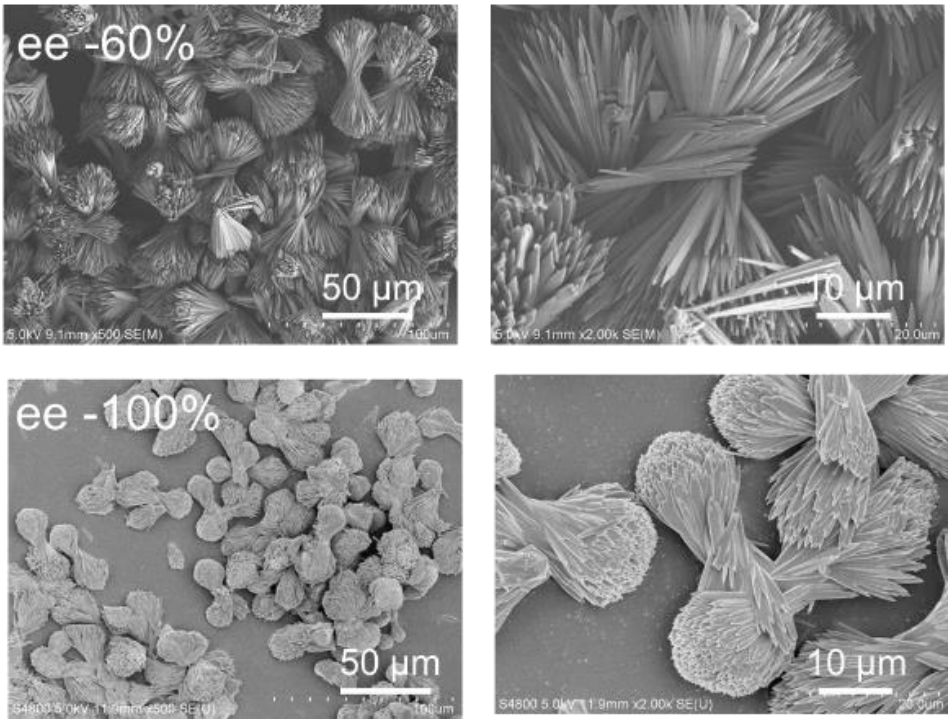

Figure S16. SEM images of the $Gd(NO_3)_3$/*R*-,*S*-$AnempH_2$ assemblies obtained in 90 vol % NPA / DMF (total volume 5 mL) and 0.5 mL water with different ratio of the *R*-$AnempH_2$/*S*-$AnempH_2$ enantiomers.

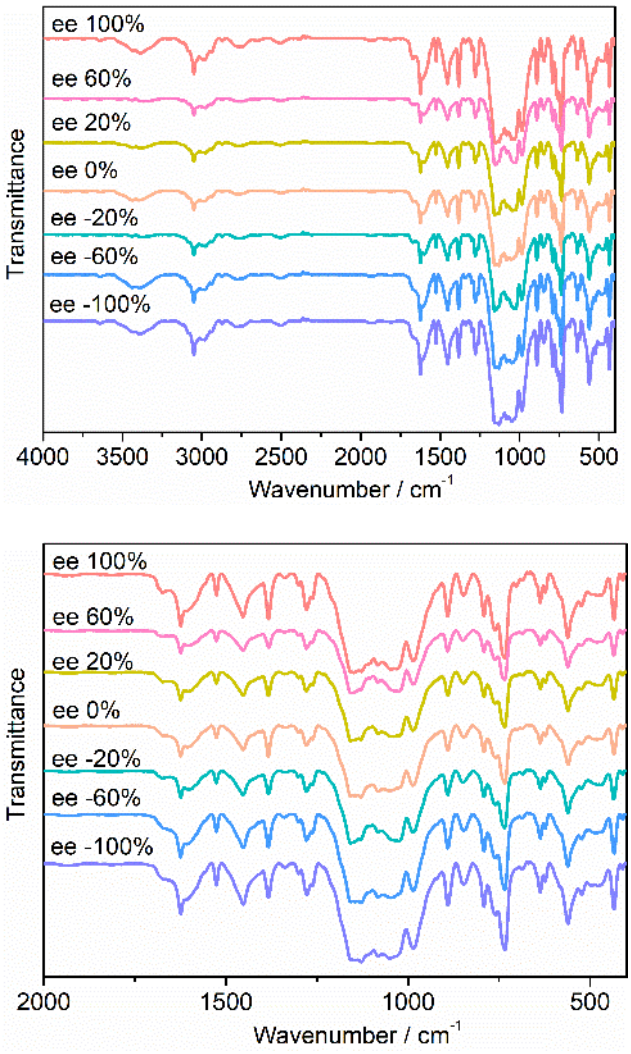

Figure S17. IR spectra of the $Gd(NO_3)_3$/*R*-,*S*-AnempH_2 assemblies obtained in 90 vol % NPA / DMF (total volume 5 mL) and 0.5 mL water with different ratio of the *R*-AnempH_2/*S*-AnempH_2 enantiomers.

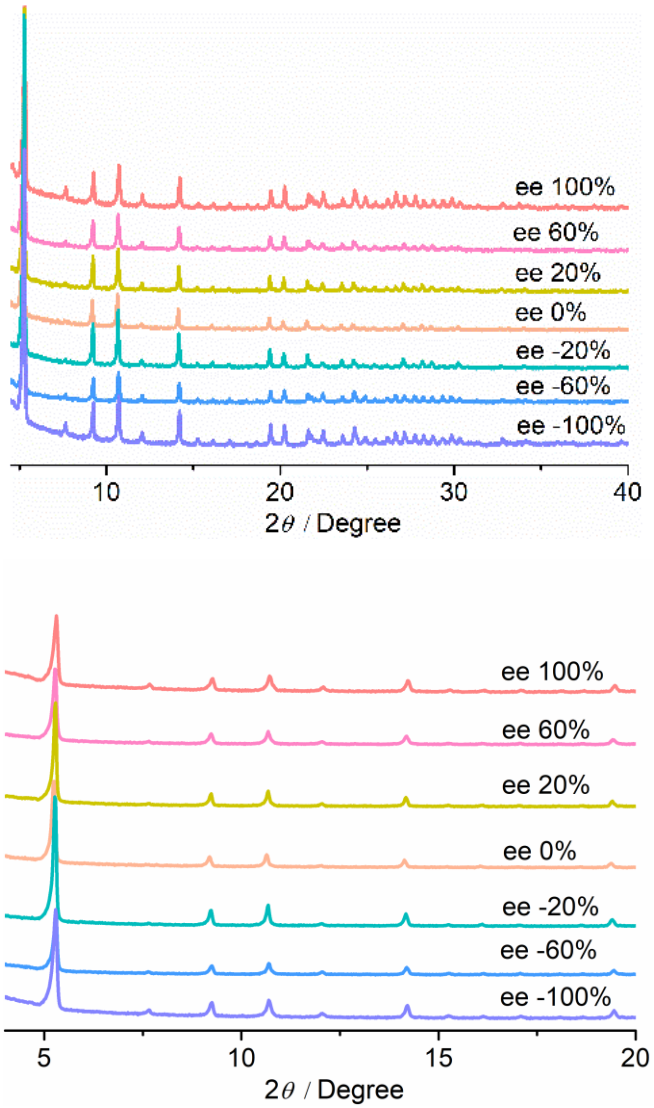

Figure S18. PXRD patterns of the $Gd(NO_3)_3$/*R*-,*S*-$AnempH_2$ assemblies obtained in 90 vol % NPA / DMF (total volume 5 mL) and 0.5 mL water with different ratio of the *R*-$AnempH_2$/*S*-$AnempH_2$ enantiomers.

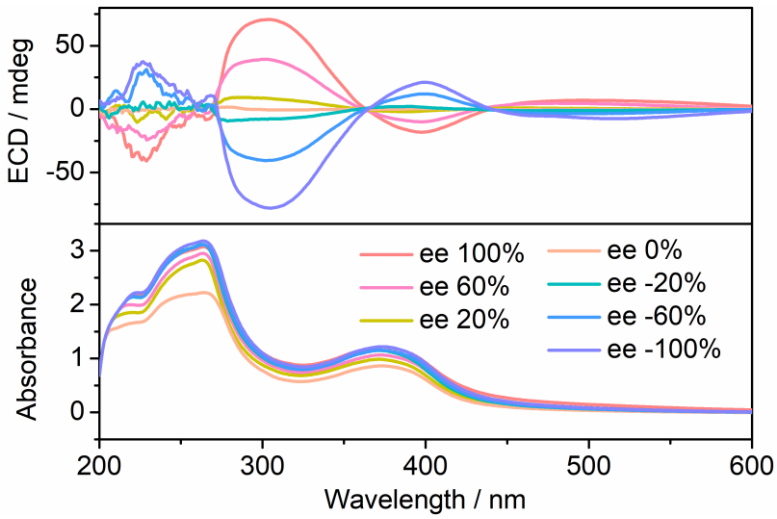

Figure S19. ECD spectra of the $Gd(NO_3)_3$/*R*-,*S*-AnempH_2 assemblies obtained in 90 vol % NPA / DMF (total volume 5 mL) and 0.5 mL water with different ratio of the *R*-AnempH_2/*S*-AnempH_2 enantiomers. The measurements were performed on a JASCO J-810 spectrophotometer.

III. The structure of *R*-2

Table S2. Selected bond lengths [Å] for ***R*-2**.

bond lengths	[Å]	bond lengths	[Å]
Gd1-O1	2.3863	Gd2-O7D	2.3138
Gd1-O3	2.5354	Gd3-O7	2.4056
Gd1-O4	2.5369	Gd3-O10	2.2674
Gd1-O1B	2.3863	Gd3-O7B	2.4056
Gd1-O3B	2.5354	Gd3-O10B	2.2674
Gd1-O4B	2.5369	Gd3-O7D	2.4056
Gd1-O1D	2.3863	Gd3-O10D	2.2674
Gd1-O3D	2.5354	Gd4-O12	2.1922
Gd1-O4D	2.5369	Gd4-O3A	2.3206
Gd2-O4	2.3018	Gd4-O12B	2.1921
Gd2-O7	2.3138	Gd4-O3C	2.3206
Gd2-O4B	2.3018	Gd4-O12D	2.1921
Gd2-O7B	2.3138	Gd4-O3E	2.3207
Gd2-O4D	2.3018		

Table S3. Selected bond angles [°] for ***R*-2**.

bond angles	[˚]	bond angles	[˚]
O1-Gd1-O3	58.12	O4B-Gd2-O7	157.17
O1-Gd1-O4	78.37	O7-Gd2-O7B	71.33
O1-Gd1-O1B	119.55	O4D-Gd2-O7	123.22
O1-Gd1-O3B	80.56	O7-Gd2-O7D	71.33
O1-Gd1-O4B	70.63	O4B-Gd2-O7B	95.59
O1-Gd1-O1D	119.55	O4B-Gd2-O4D	75.62
O1-Gd1-O3D	122.3	O4B-Gd2-O7D	123.22
O1-Gd1-O4D	133.48	O4D-Gd2-O7B	157.17
O3-Gd1-O4	103.83	O7B-Gd2-O7D	71.33
O1B-Gd1-O3	122.3	O4D-Gd2-O7D	95.59
O3-Gd1-O3B	65.52	O7-Gd3-O10	109.99
O3-Gd1-O4B	128.56	O7-Gd3-O7B	68.22
O1D-Gd1-O3	80.56	O7-Gd3-O10B	78.02
O3-Gd1-O3D	65.52	O7-Gd3-O7D	68.22
O3-Gd1-O4D	158.88	O7-Gd3-O10D	144.33
O1B-Gd1-O4	133.48	O7B-Gd3-O10	144.33
O3B-Gd1-O4	158.88	O10-Gd3-O10B	104.05
O4-Gd1-O4B	67.6	O7D-Gd3-O10	78.02
O1D-Gd1-O4	70.63	O10-Gd3-O10D	104.05
O3D-Gd1-O4	128.56	O7B-Gd3-O10B	109.99

bond angles	[˚]	bond angles	[˚]
O4-Gd1-O4D	67.6	O7B-Gd3-O7D	68.22
O1B-Gd1-O3B	58.12	O7B-Gd3-O10D	78.02
O1B-Gd1-O4B	78.37	O7D-Gd3-O10B	144.33
O1B-Gd1-O1D	119.55	O10B-Gd3-O10D	104.05
O1B-Gd1-O3D	80.56	O7D-Gd3-O10D	109.99
O1B-Gd1-O4D	70.63	O3A-Gd4-O12	138.17
O3B-Gd1-O4B	103.83	O12-Gd4-O12B	91.71
O1D-Gd1-O3B	122.3	O3C-Gd4-O12	129.43
O3B-Gd1-O3D	65.52	O12-Gd4-O12D	91.71
O3B-Gd1-O4D	128.56	O3E-Gd4-O12	81.2
O1D-Gd1-O4B	133.48	O3A-Gd4-O12B	81.2
O3D-Gd1-O4B	158.88	O3A-Gd4-O3C	72.49
O4B-Gd1-O4D	67.6	O3A-Gd4-O12D	129.43
O1D-Gd1-O3D	58.12	O3A-Gd4-O3E	72.49
O1D-Gd1-O4D	78.37	O3C-Gd4-O12B	138.17
O3D-Gd1-O4D	103.83	O12B-Gd4-O12D	91.71
O4-Gd2-O7	95.59	O3E-Gd4-O12B	129.43
O4-Gd2-O4B	75.62	O3C-Gd4-O12D	81.2
O4-Gd2-O7B	123.22	O3C-Gd4-O3E	72.49
O4-Gd2-O4D	75.62	O3E-Gd4-O12D	138.17
O4-Gd2-O7D	157.17		

Symmetry Code: A x, y,1+z; B 1-y,1+x-y, z; C 1-y,1+x-y,1+z; D -x+y,1-x, z; E -x+y,1-x,1+z

Table S4. Hydrogen bonds in ***R*-2**.

D-H···A	d(D-H) [Å]	d(H···A) [Å]	d(D···A) [Å]	<DHA [°]
N1-H3...O3	1.04	1.97	2.6960	124
N1-H4 …O6	1.33	1.18	2.4967	171
N2- H19...O9	1.10	1.5	2.5896	172
N2-H20...O1	1.08	1.53	2.5712	160
N3-H33...O10	1.05	1.88	2.8828	158
N3-H34...O5	1.09	1.51	2.5638	161
N4-H51...O8	1.12	1.43	2.5252	164
N4-H181...O12	1.04	2.28	2.8907	116

Table S5. C-H···π interactions in ***R*-2**.

	C-H···π [°]	d(H···π) [Å]	d(C···π) [Å]
C26-H27···π	150	2.85	3.8332
C28-H28···π	159	2.76	3.7610
C30-H29···π	169	2.72	3.7980

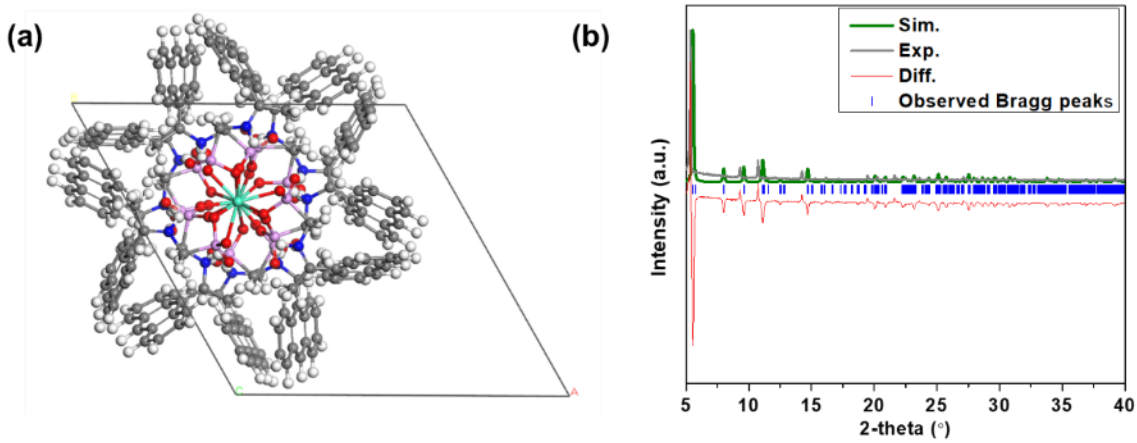

Figure S20. The optimized crystal structure and PXRD simulation results of ***R*-2**.

The ***R*-2*** simulated models were optimized using the Perdew-Burke-Ernzerh (PBE)[1] functional within the Vienna Ab initio Simulation Package (VASP).[2] A plane-wave basis set with a cut-off energy of 450 eV was employed. Convergence thresholds for energy and force were established at 1×10^{-5} eV and -0.02 eV $Å^{-1}$, respectively, as demonstrated in Figure S19a.

For PXRD simulations, we utilized the Powder Refinement feature in the Reflex module of Materials Studio software.[3] Peak shapes were fitted using the Pseudo-Voigt function, with FWHM parameters set to U = 0.22, V = -0.16, and W = 0.03. PXRD simulations were conducted by comparing the calculated spectra (green lines) with the experimental data (gray lines) of ***R*-2***, shown in Figure S19b, revealing a slight rightward shift of the peaks.

References:

(1) John, P.; Perdew, K. B.; Matthias, E. Generalized Gradient Approximation Made Simple. Phys. Rev. Lett. 1996, 77, 3865-3868.

(2) Kresse, G.; Furthmüller, J. Efficiency of ab-initio total energy calculations for metals and semiconductors using a plane-wave basis set. Comput. Mater. Sci. 1996, 6, 15-50.

(3) Materials Studio, version 7.0; Accelrys Inc.: San Diego, 2013.

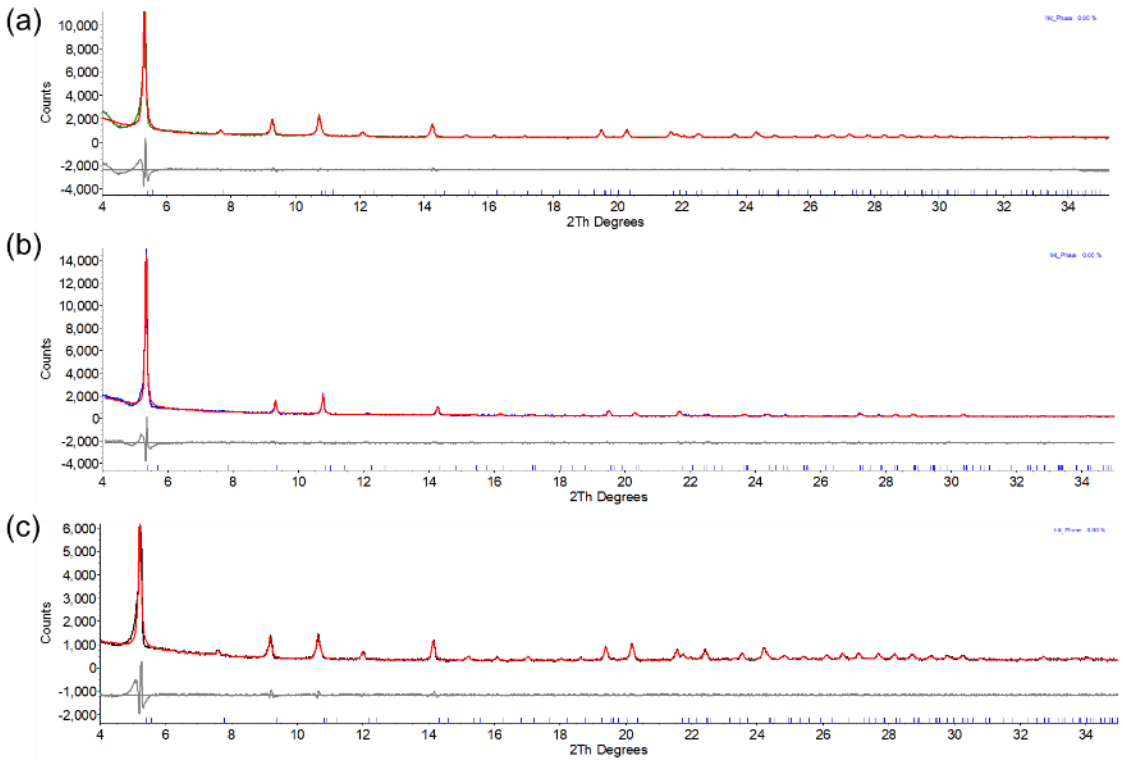

Figure S21. Pawley fits of powder samples of ***R*-1** (a), ***R*-2** (b), ***R*-3** (c) performed using Topas 5.0 program.

Fitted cell parameters for ***R*-1**: *P*3, *a* = 18.85 Å, *c* = 15.82 Å, *V* = 4870.24 Å^3, Rwp 9.295;

Fitted cell parameters for ***R*-2**: *P*3, *a* = 18.86 Å, *c* = 15.29 Å, *V* = 4764.21 Å^3, Rwp 9.937;

Fitted cell parameters for ***R*-3**: *P*3, *a* = 18.87 Å, *c* = 15.80 Å, *V* = 4872.6 Å^3, Rwp 8.09.

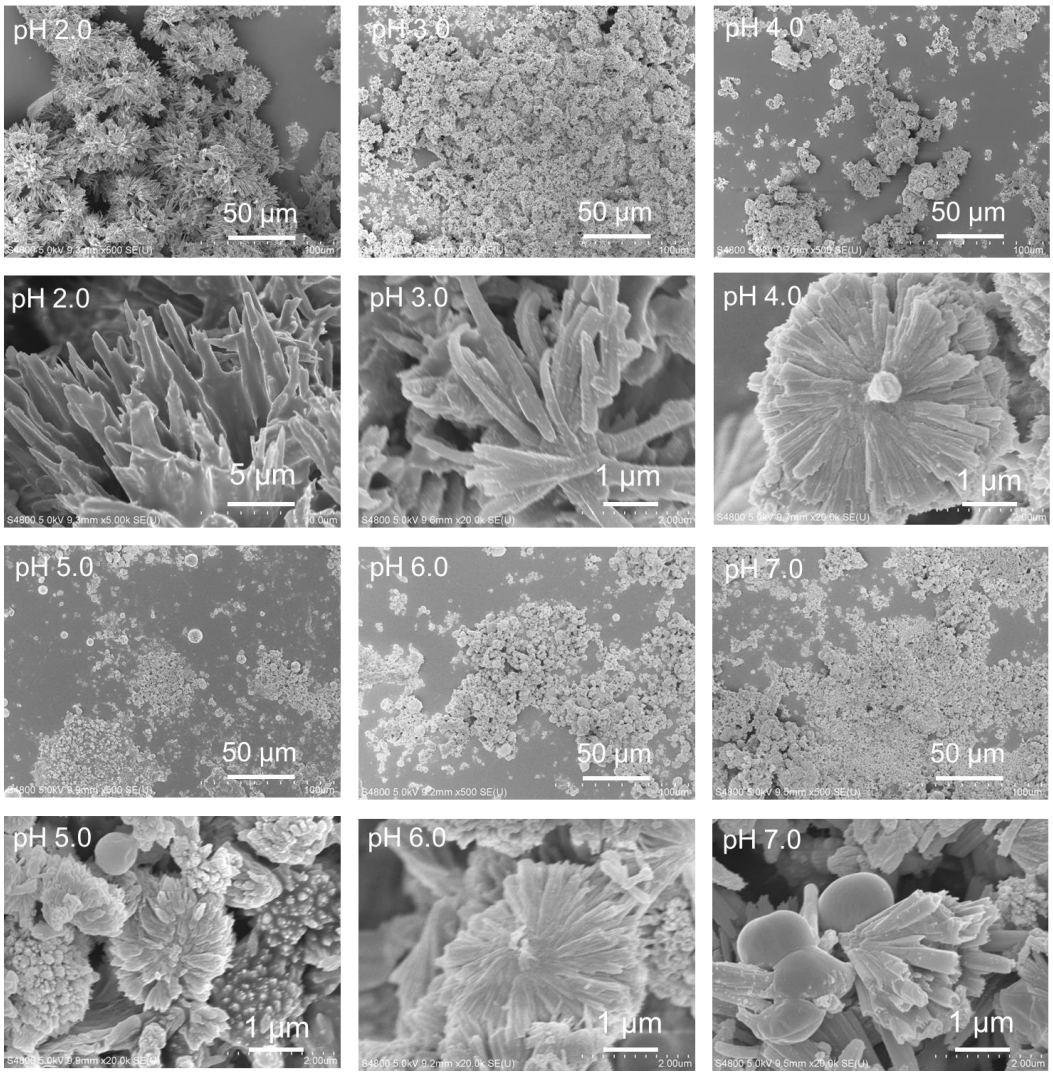

Figure S22. SEM images showing the morphology of the $Gd(NO_3)_3$/*R*-AnempH_2 assemblies obtained at different pH under hydrothermal conditions at 120°C for 24h.

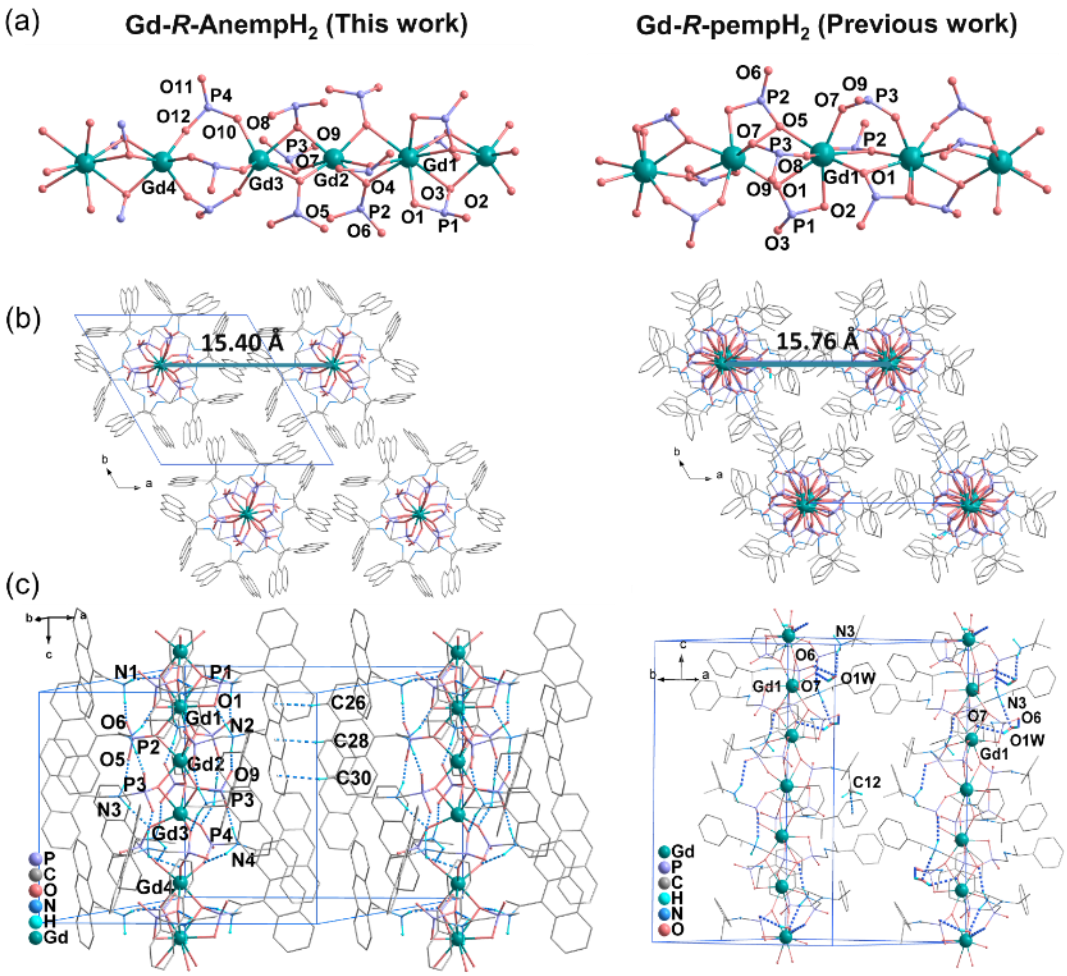

Figure S23. The structure of ***R*-2** (left) and Gd(*R*-pempH)$_3$·1.5H$_2$O (right). (a) the fragment of the chain structure in ***R*-2** and Gd(*R*-pempH)$_3$·1.5H$_2$O, ball and stick representation with atomic labelling. All C and N atoms are omitted for clarity. (b) interchain distances and (c) packing diagrams of structures of ***R*-2** and Gd(*R*-pempH)$_3$·1.5H$_2$O. The dotted lines represent the hydrogen bonding interactions and C-H…π interaction. The structure of Gd(*R*-pempH)$_3$·1.5H$_2$O is adapted from ref..

IV. The influence of reaction conditions on the spiral bundles

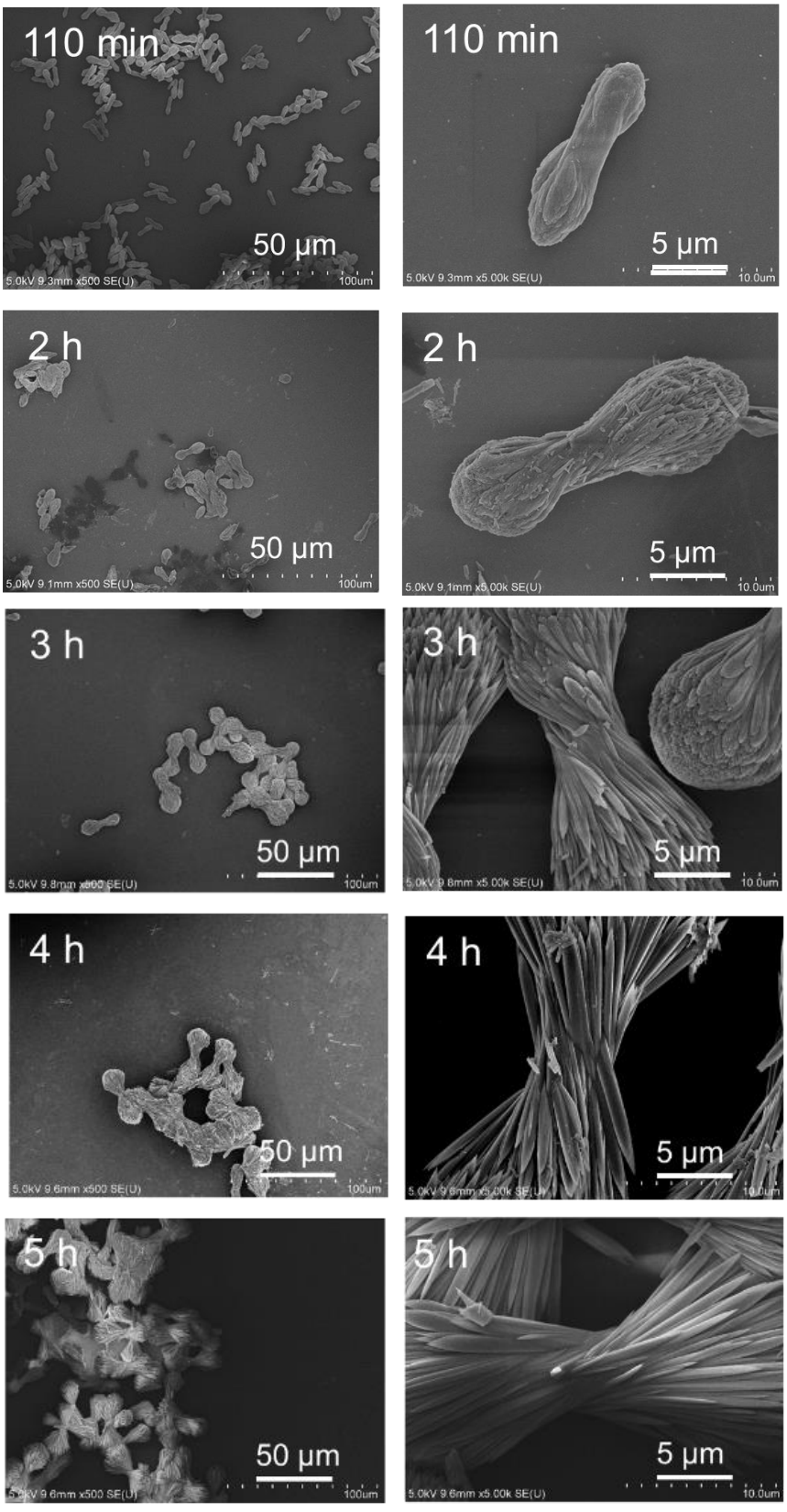

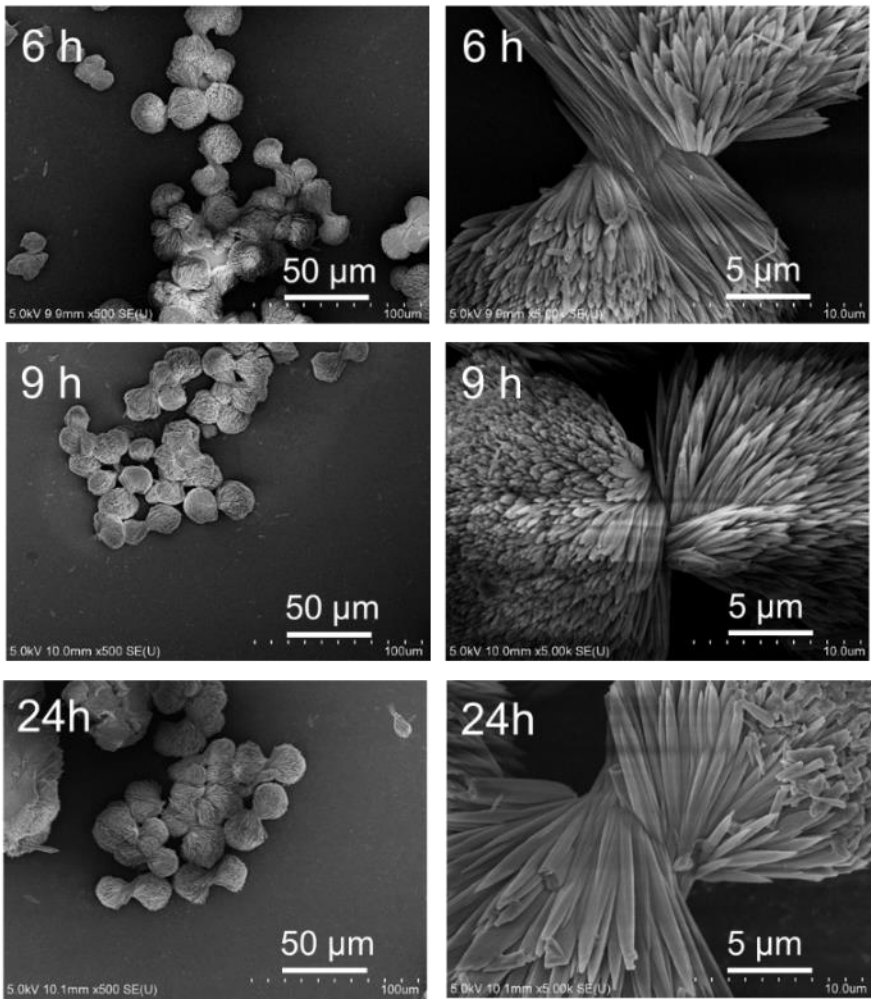

Figure S24. SEM images showing the morphology of the $Gd(NO_3)_3$/*R*-AnempH_2 assemblies obtained in 90 vol % NPA / DMF (total volume 5 mL) and 0.5 mL water after reaction for different period of time.

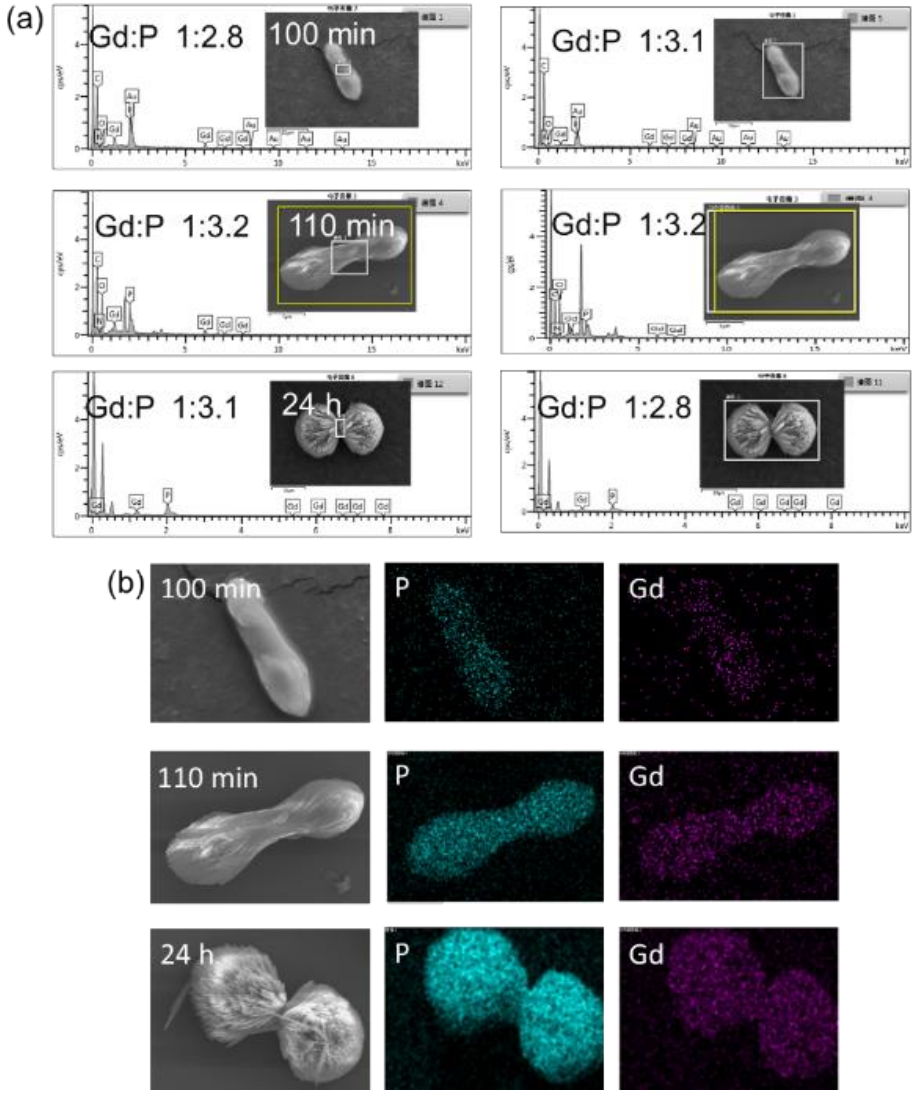

Figure S25. (a) EDS result and (b) mapping images of the $Gd(NO_3)_3$/*R*-AnempH_2 assemblies obtained in 90 vol % NPA / DMF (total volume 5 mL) and 0.5 mL water after reaction for different period of time.

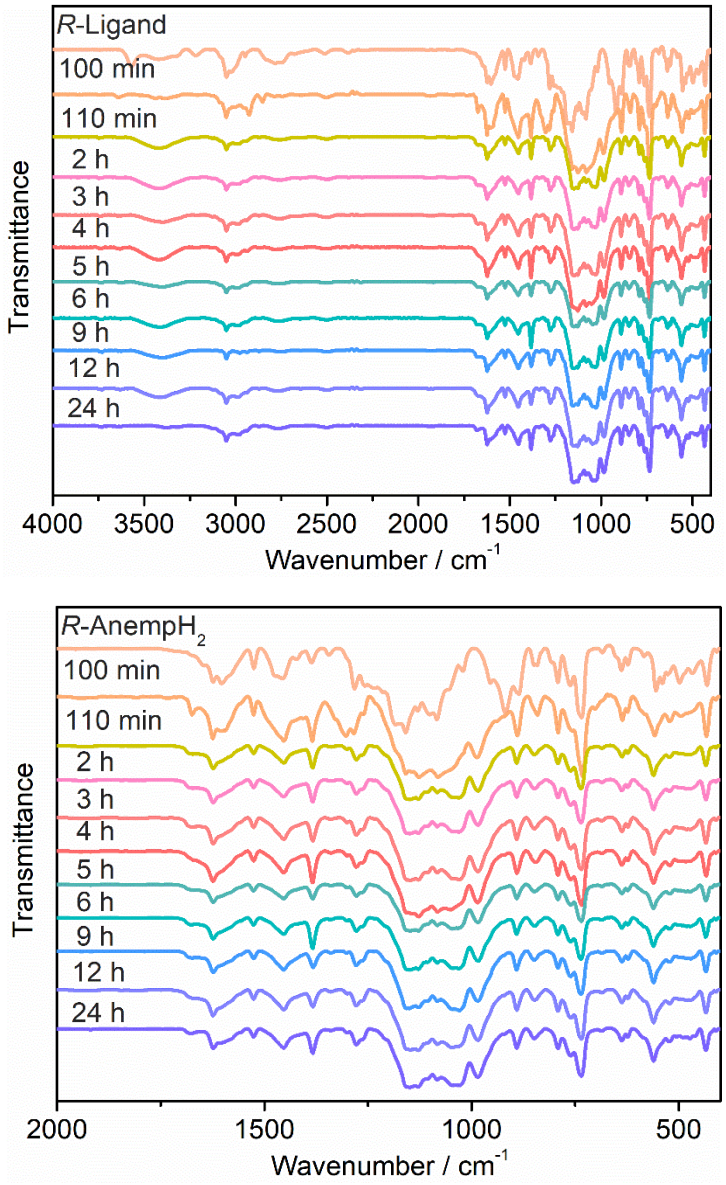

Figure S26. IR spectra of the $Gd(NO_3)_3$/*R*-AnempH_2 assemblies obtained in 90 vol % NPA / DMF (total volume 5 mL) and 0.5 mL water after reaction for different period of time. up: 4000-400 cm^{-1}, bottom: 2000-400 cm^{-1}.

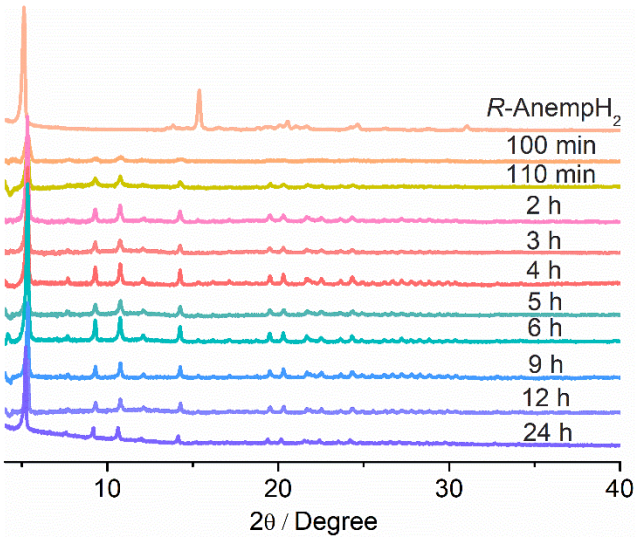

Figure S27. PXRD patterns of the $Gd(NO_3)_3$/*R*-$AnempH_2$ assemblies obtained in 90 vol % NPA / DMF (total volume 5 mL) and 0.5 mL water after reaction for different period of time.

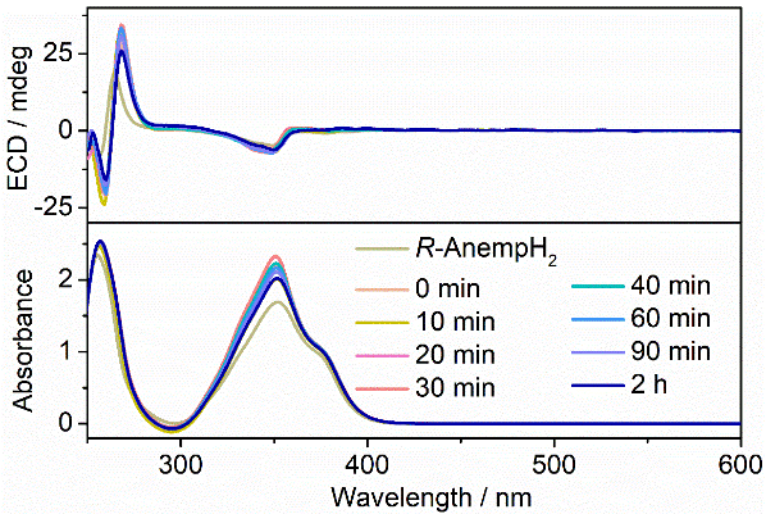

Figure S28. ECD spectra of the solutions after reacting $Gd(NO_3)_3$ with *R*-$AnempH_2$ in 90 vol % NPA / DMF (total volume 5 mL) and 0.5 mL water for different period of time. The measurements were performed on a JASCO J-810 spectrophotometer.

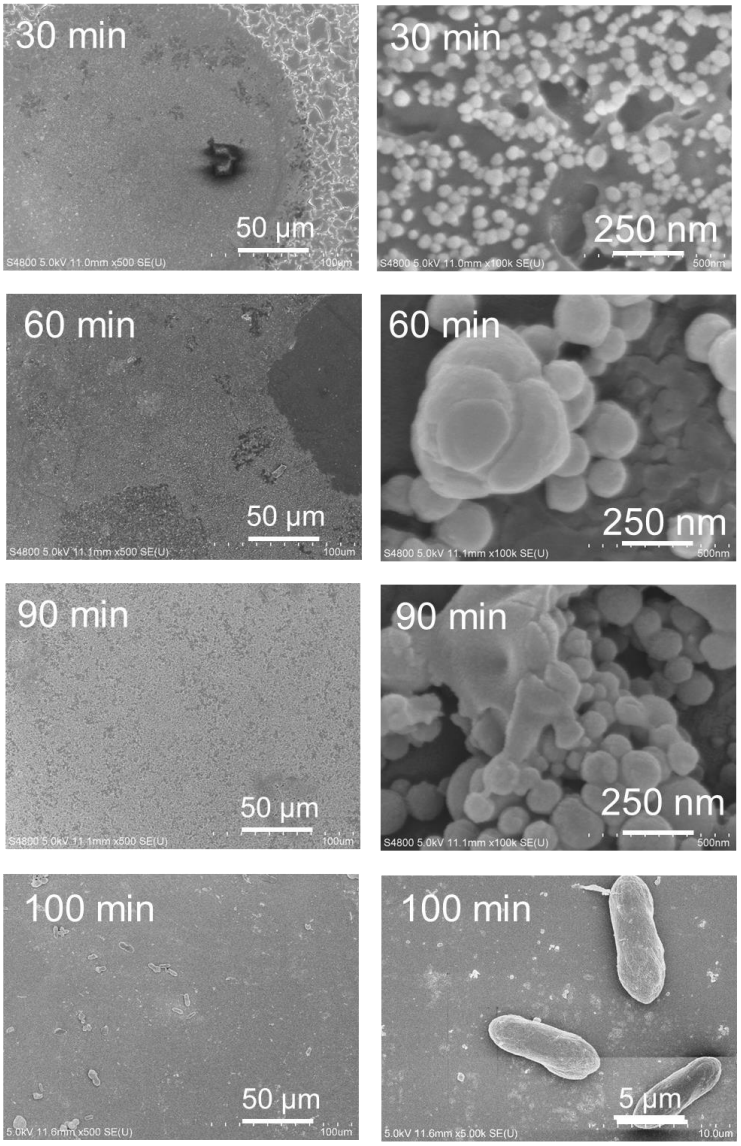

Figure S29. SEM images showing the morphology of products at different reaction time.

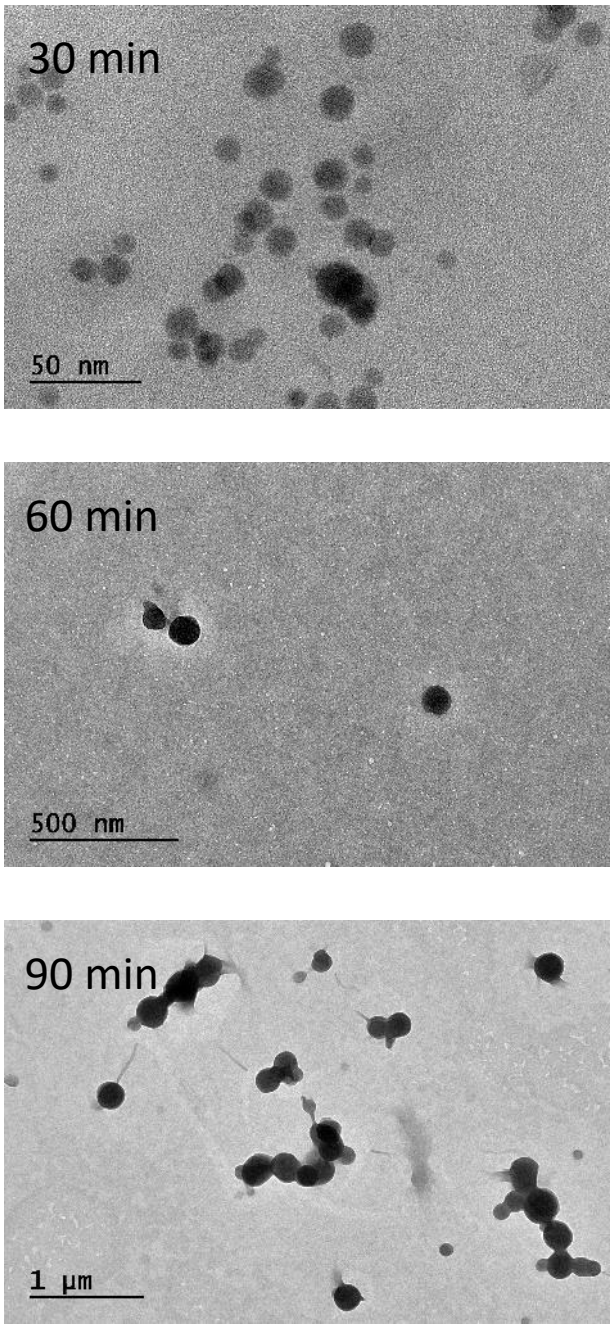

Figure S30. TEM images showing the morphology of products at different reaction time.

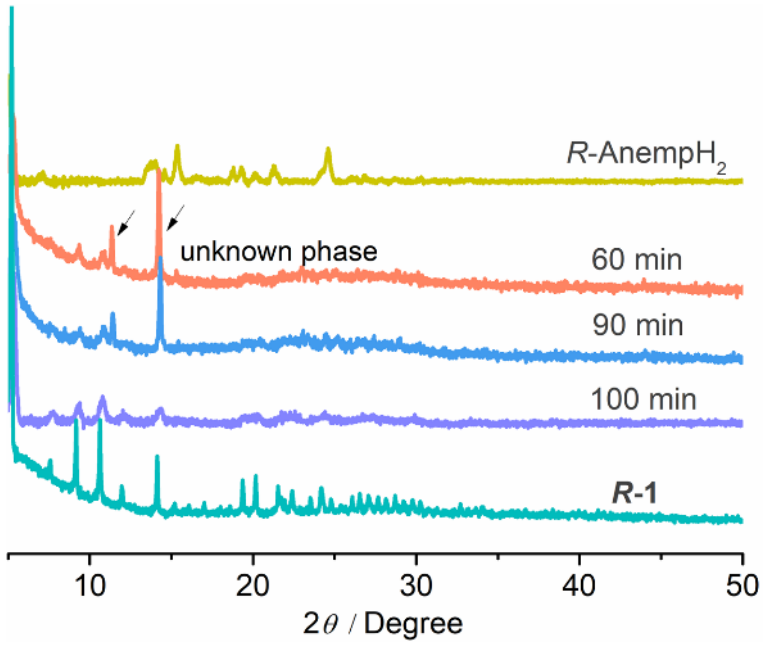

Figure S31. PXRD patterns of the residues after solvent evaporation of the reaction solutions at different reaction time.

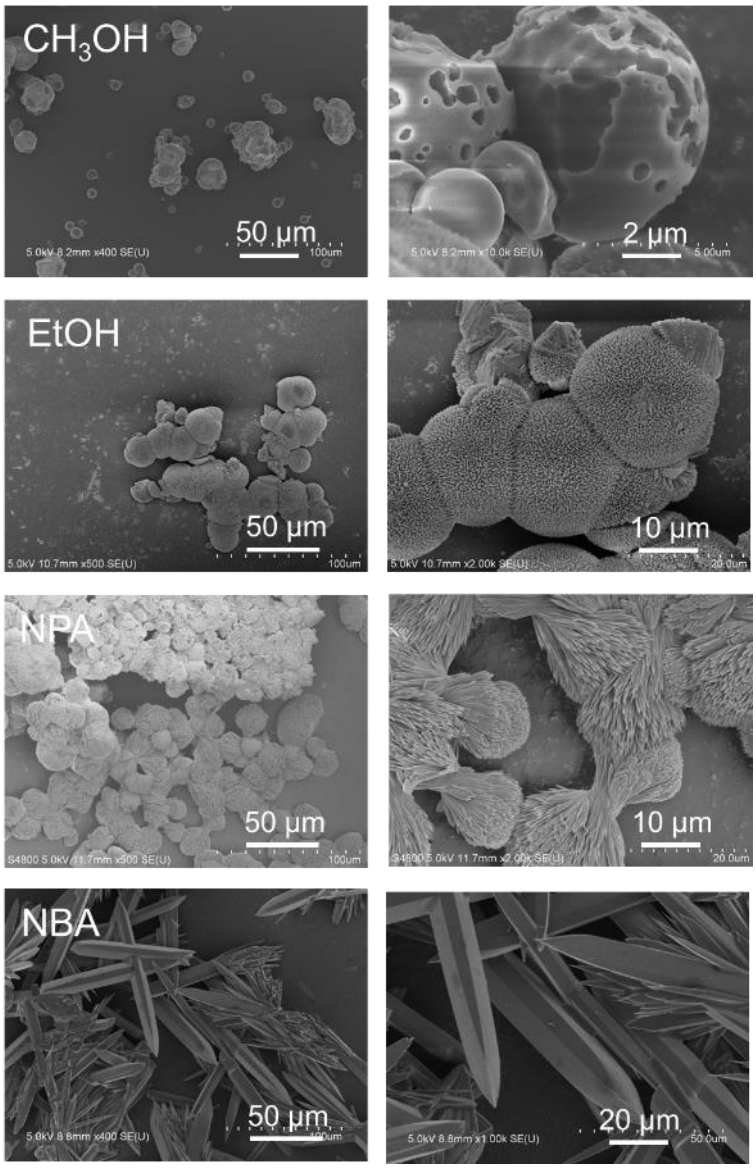

Figure S32. SEM images showing the morphology of the $Gd(NO_3)_3$/*R*-AnempH_2 (1:3) assemblies obtained in 90 vol % alcohol / DMF (total volume 5 mL) and 0.5 mL water at 100°C using different alcohol (CH_3OH, EtOH, NPA, NBA).

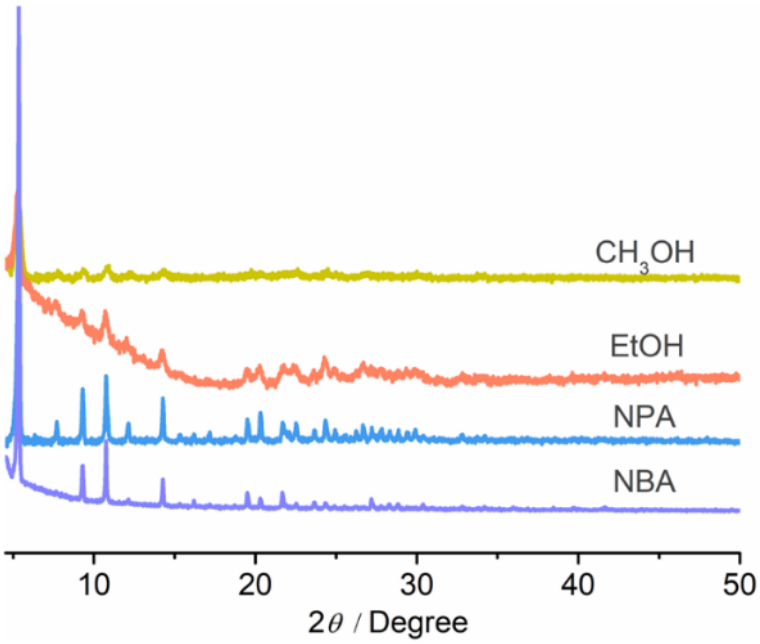

Figure S33. PXRD patterns of the $Gd(NO_3)_3$/*R*-AnempH_2 (1:3) assemblies obtained in 90 vol % alcohol / DMF (total volume 5 mL) and 0.5 mL water at 100°C using different alcohol (CH_3OH, EtOH, NPA, NBA).

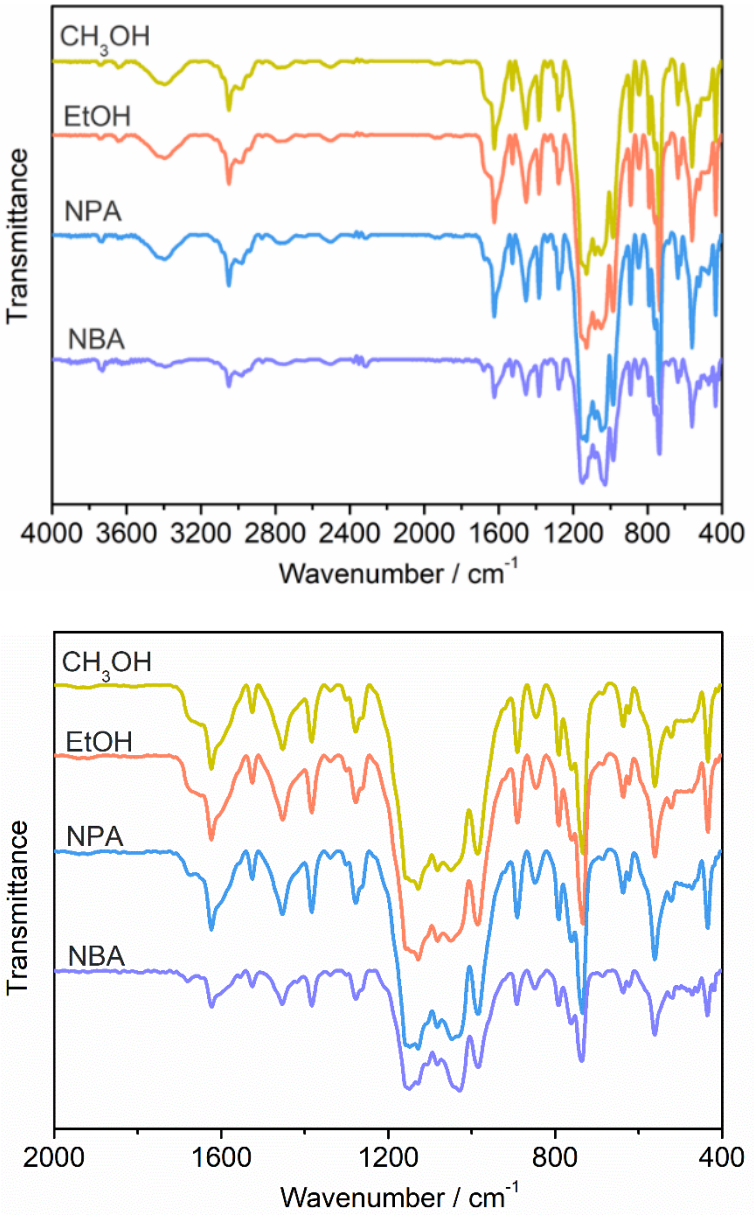

Figure S34. IR spectra of the $Gd(NO_3)_3$/*R*-AnempH_2 (1:3) assemblies obtained in 90 vol % alcohol / DMF (total volume 5 mL) and 0.5 mL water at 100°C using different alcohol (CH_3OH, EtOH, NPA, NBA). Up: 4000-400 cm^{-1}, bottom: 2000-400 cm^{-1}.

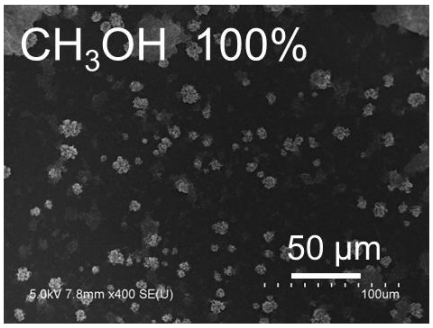
CH3OH 100%
50 µm
5.0kV 7.8mm x400 SE(U)
100um

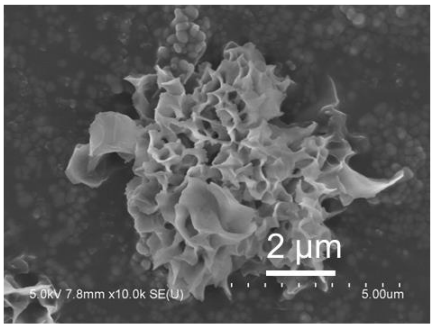
2 µm
5.0kV 7.8mm x10.0k SE(U)
5.00um

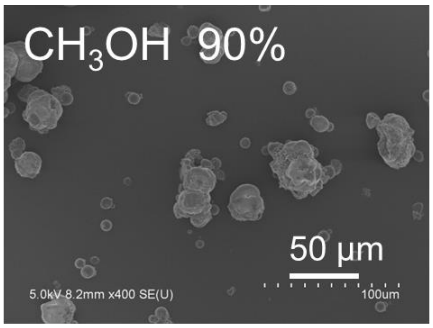
CH3OH 90%
50 µm
5.0kV 8.2mm x400 SE(U)
100um

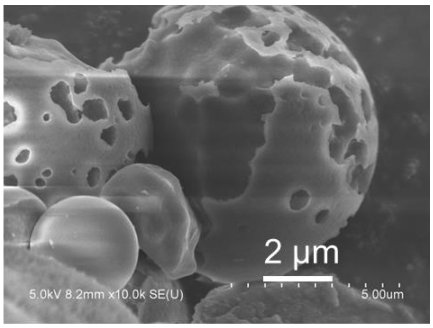
2 µm
5.0kV 8.2mm x10.0k SE(U)
5.00um

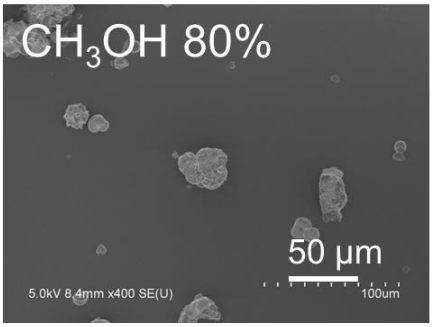
CH3OH 80%
50 µm
5.0kV 8.4mm x400 SE(U)
100um

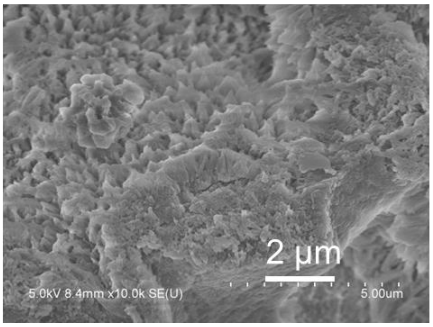
2 µm
5.0kV 8.4mm x10.0k SE(U)
5.00um

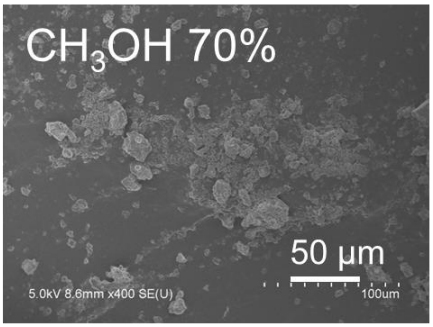
CH3OH 70%
50 µm
5.0kV 8.6mm x400 SE(U)
100um

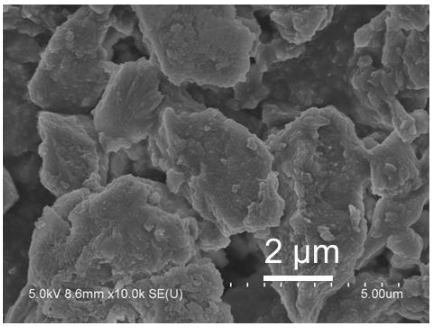
2 µm
5.0kV 8.6mm x10.0k SE(U)
5.00um

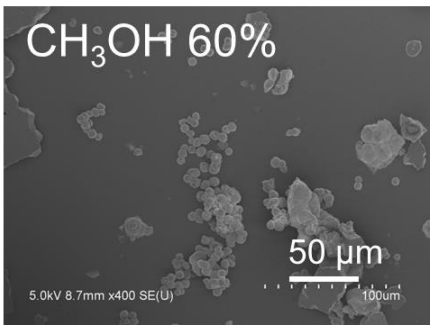
CH3OH 60%
50 µm
5.0kV 8.7mm x400 SE(U)
100um

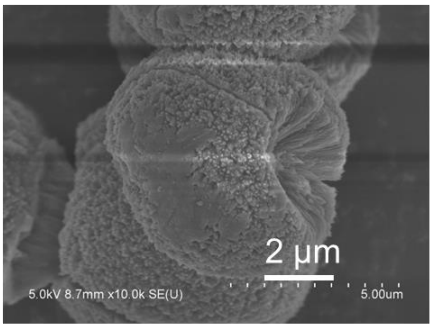
2 µm
5.0kV 8.7mm x10.0k SE(U)
5.00um

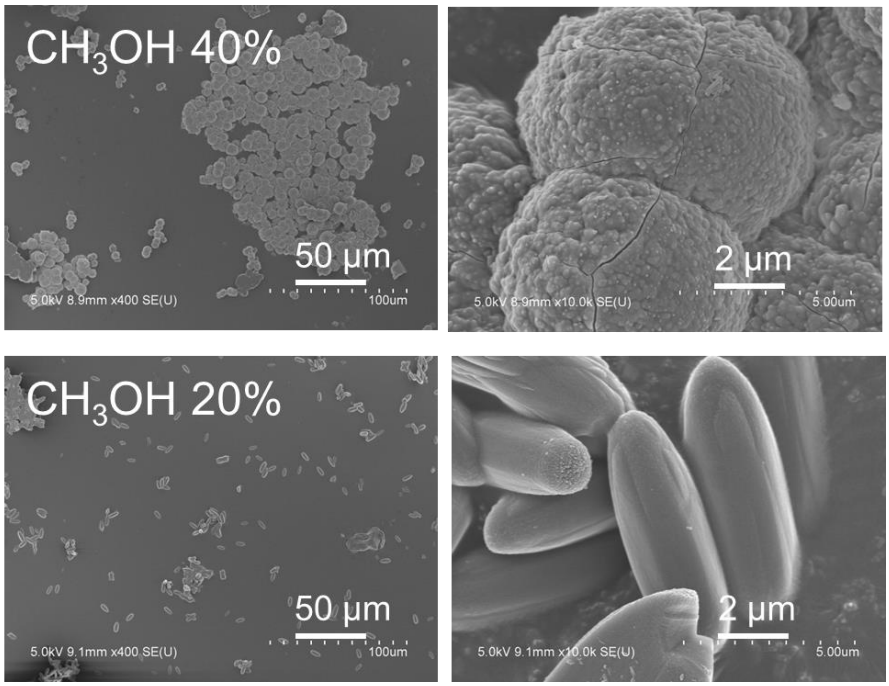

Figure S35. SEM images showing the morphology of the $Gd(NO_3)_3$/*R*-AnempH_2 (1:3) assemblies obtained in different volume ratio of CH_3OH / DMF (total volume 5 mL) and 0.5 mL water at 100°C.

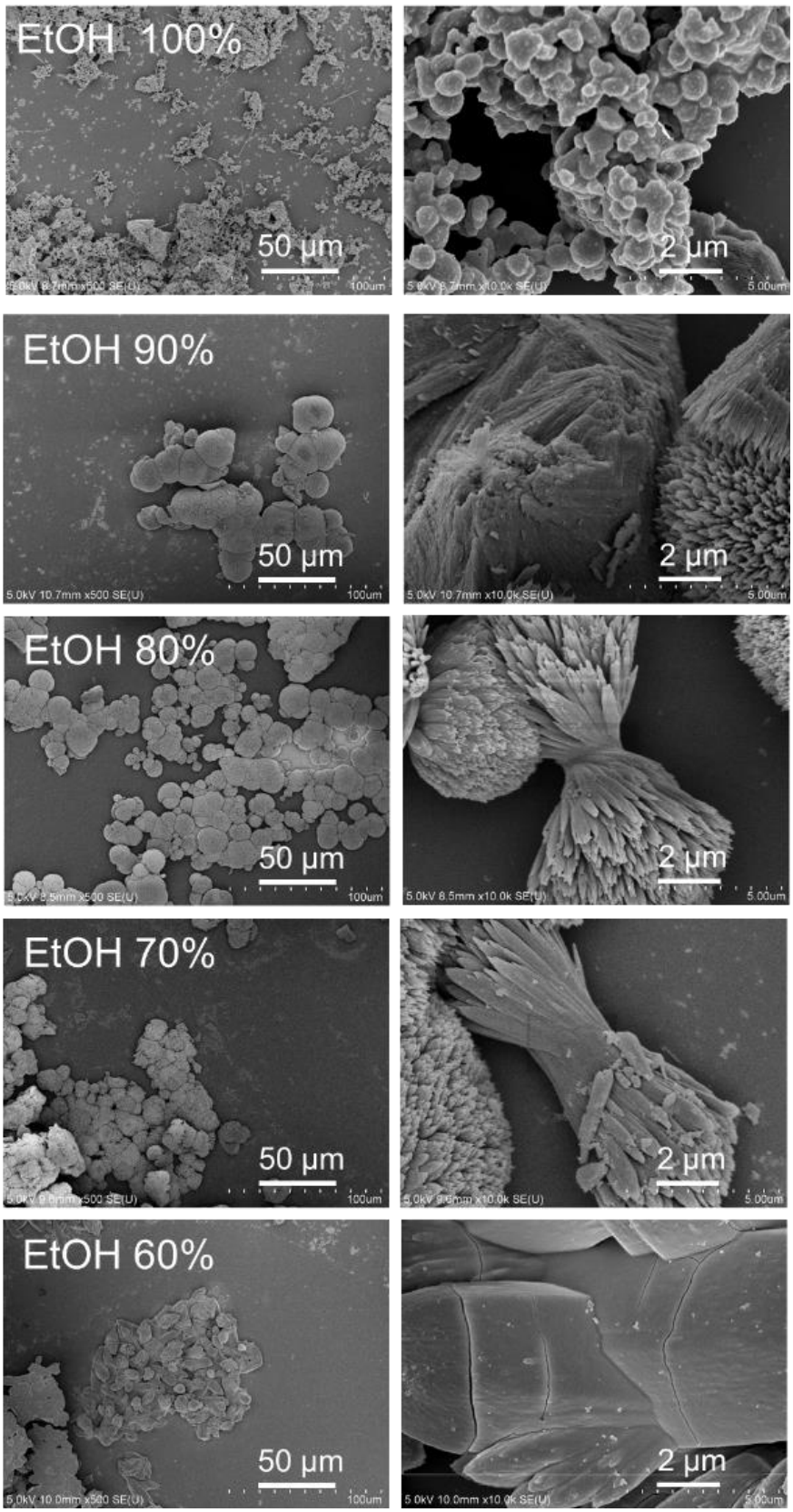
EtOH 100%
50 µm
2 µm
EtOH 90%
50 µm
2 µm
EtOH 80%
50 µm
2 µm
EtOH 70%
50 µm
2 µm
EtOH 60%
50 µm
2 µm

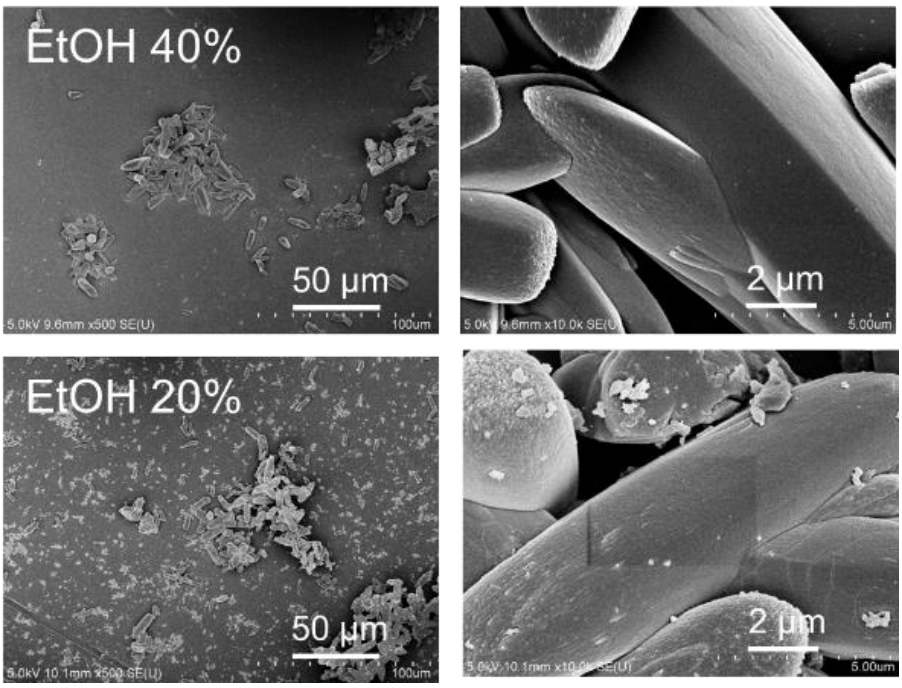

Figure S36. SEM images showing the morphology of the $Gd(NO_3)_3$/*R*-AnempH_2 (1:3) assemblies obtained in different volume ratio of EtOH / DMF (total volume 5 mL) and 0.5 mL water at 100°C.

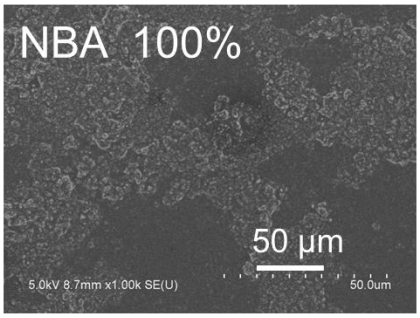
NBA 100%
50 µm
5.0kV 8.7mm x1.00k SE(U)
50.0um

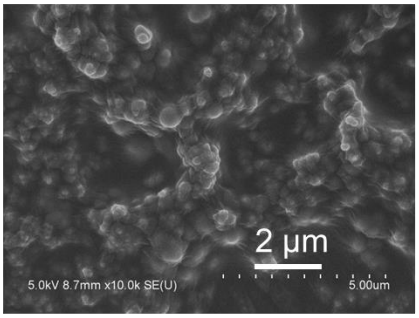
2 µm
5.0kV 8.7mm x10.0k SE(U)
5.00um

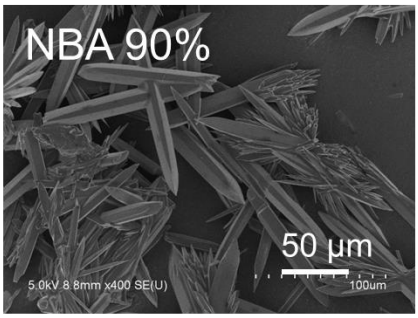
NBA 90%
50 µm
5.0kV 8.8mm x400 SE(U)
100um

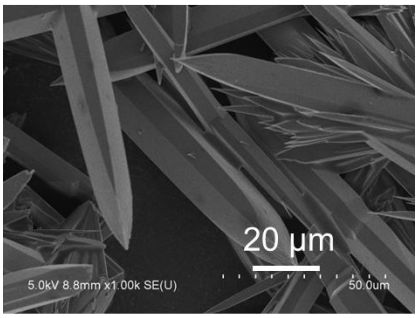
20 µm
5.0kV 8.8mm x1.00k SE(U)
50.0um

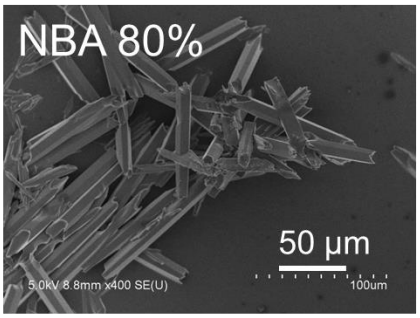
NBA 80%
50 µm
5.0kV 8.8mm x400 SE(U)
100um

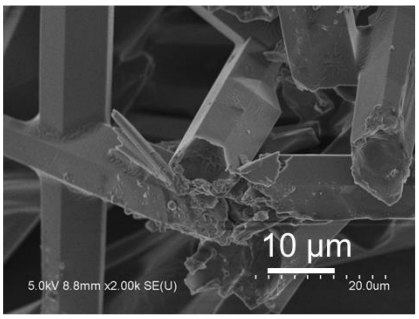
10 µm
5.0kV 8.8mm x2.00k SE(U)
20.0um

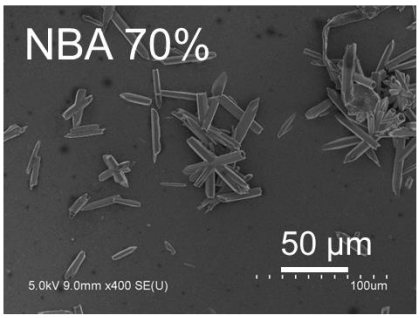
NBA 70%
50 µm
5.0kV 9.0mm x400 SE(U)
100um

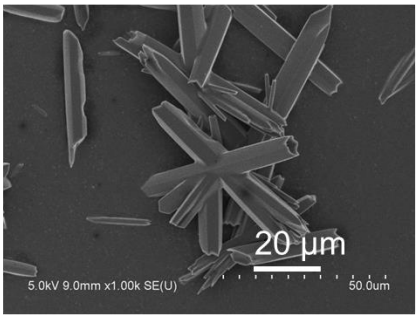
20 µm
5.0kV 9.0mm x1.00k SE(U)
50.0um

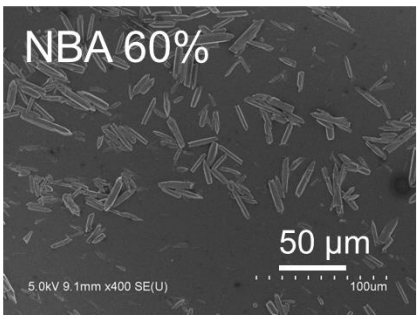
NBA 60%
50 µm
5.0kV 9.1mm x400 SE(U)
100um

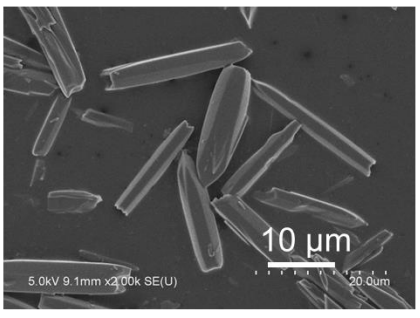
10 µm
5.0kV 9.1mm x2.00k SE(U)
20.0um

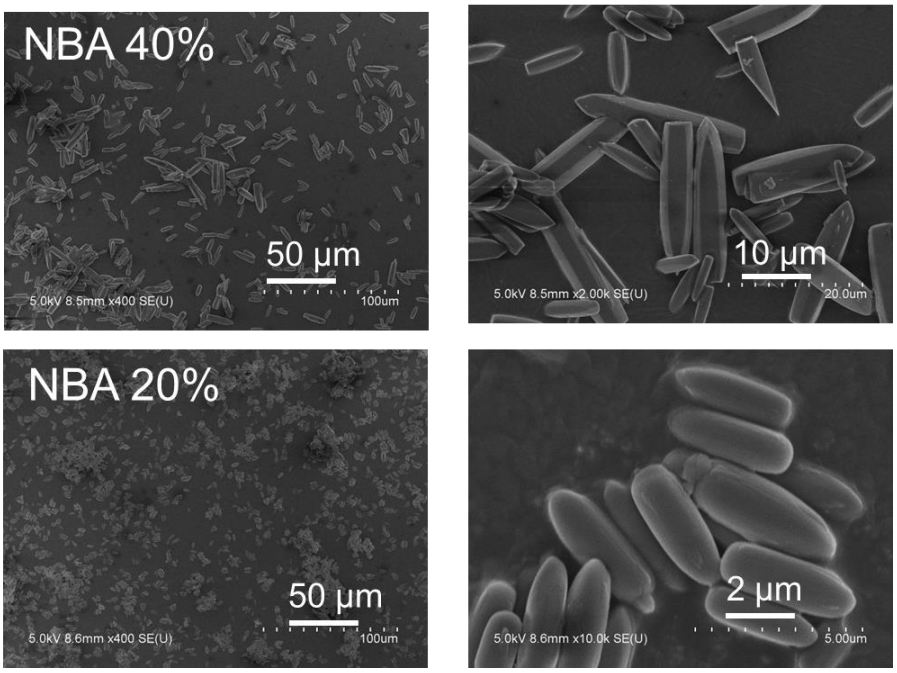

Figure S37. SEM images showing the morphology of the $Gd(NO_3)_3$/*R*-AnempH_2 (1:3) assemblies obtained in different volume ratio of NBA / DMF (total volume 5 mL) and 0.5 mL water at 100°C.

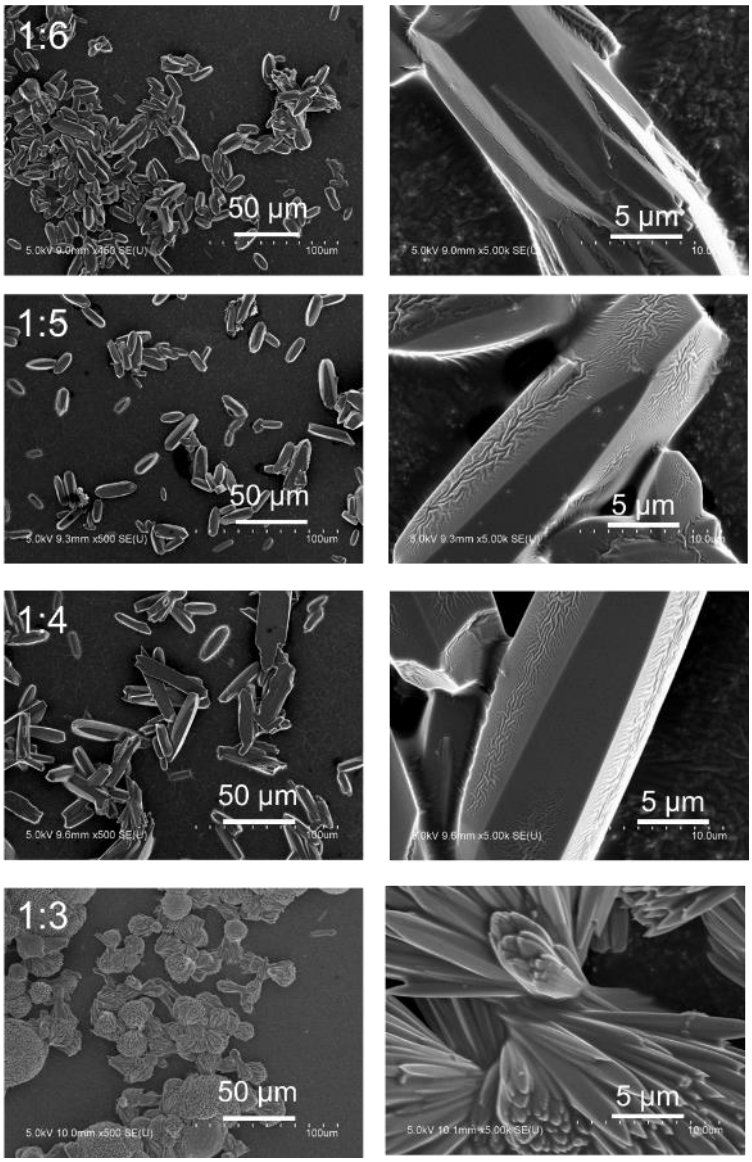

Figure S38. SEM images showing the morphology of the $Gd(NO_3)_3$/*R*-AnempH_2 assemblies with different molar ratios (1:6, 1:5, 1:4, 1:3) obtained in 90 vol % NPA / DMF (total volume 5 mL) and 0.5 mL water at 100°C.

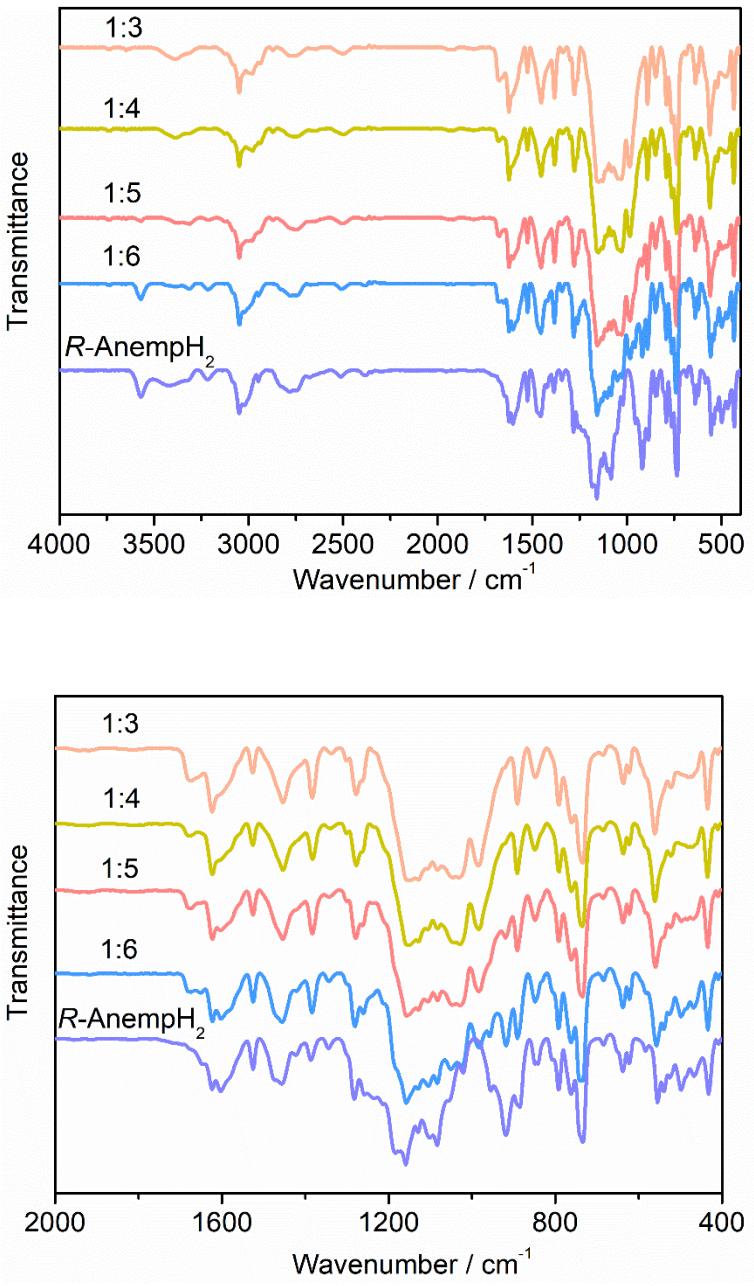

Figure S39. IR spectra of the $Gd(NO_3)_3$/*R*-AnempH_2 assemblies with different molar ratios (1:6, 1:5, 1:4, 1:3) obtained in 90 vol % NPA / DMF (total volume 5 mL) and 0.5 mL water at 100°C. Up: 4000-400 cm^{-1}, bottom: 2000-400 cm^{-1}. When ligands were in excess (1:5 and1:6), there appear peaks at 1603 cm^{-1}, 1200-800 cm^{-1}, and 464 cm^{-1} corresponding to the unreacted ligands.

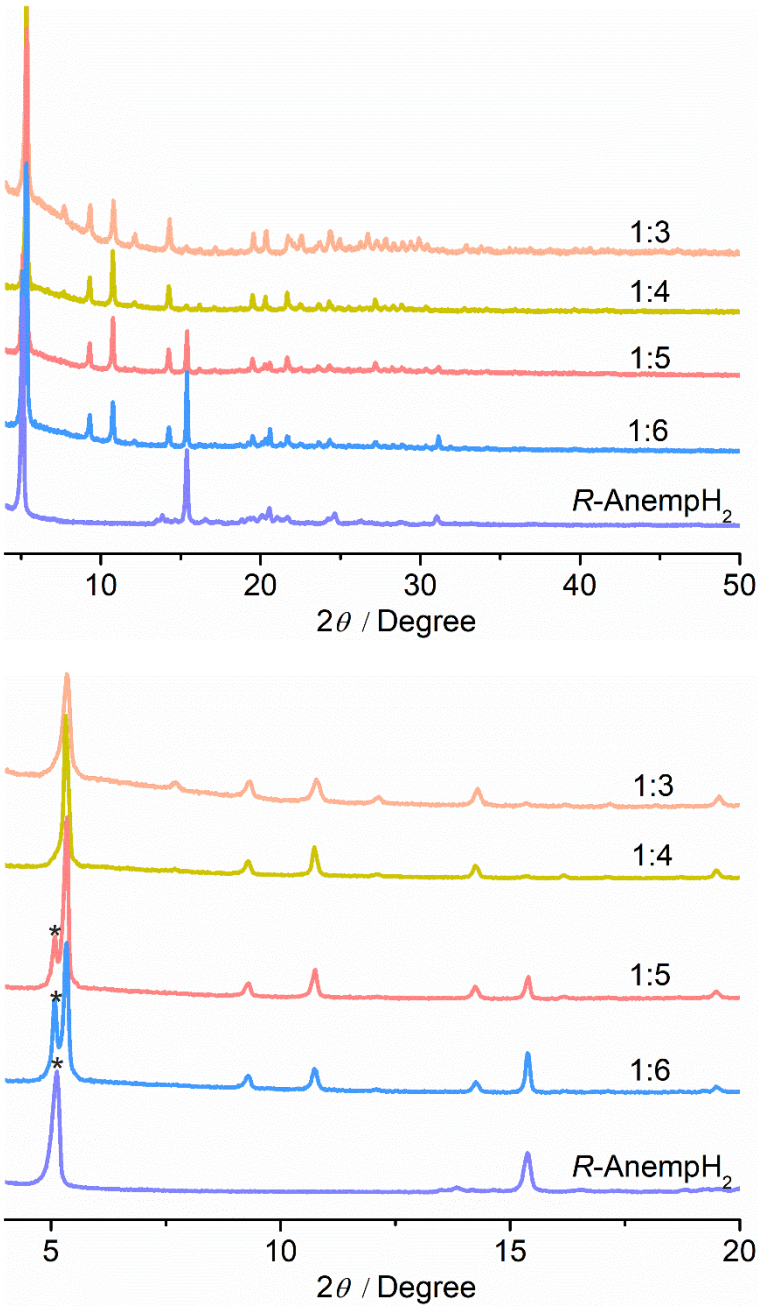

Figure S40. PXRD patterns of the $Gd(NO_3)_3$/*R*-AnempH_2 assemblies with different molar ratios (1:6, 1:5, 1:4, 1:3) obtained in 90 vol % NPA / DMF (total volume 5 mL) and 0.5 mL water at 100°C (up: 2θ 4-50°, bottom: 2θ 4-20°).

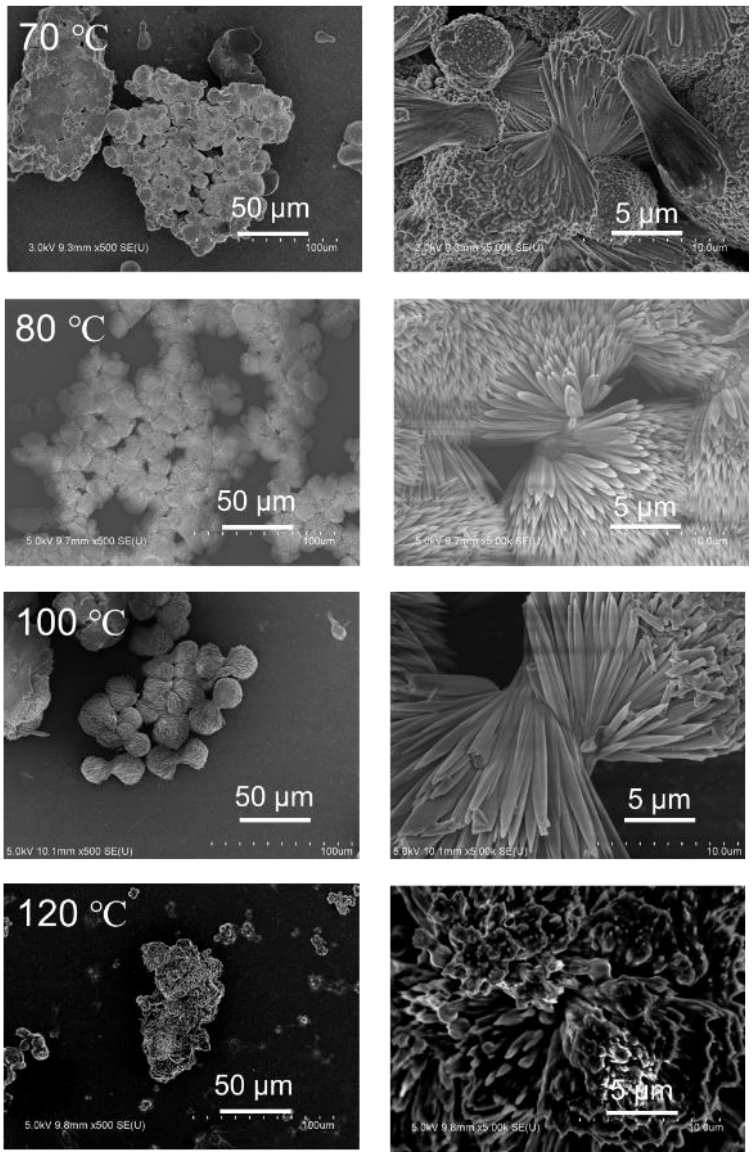

Figure S41. SEM images showing the morphology of the $Gd(NO_3)_3$/*R*-AnempH_2 (1:3) assemblies obtained in 90 vol % NPA / DMF (total volume 5 mL) and 0.5 mL water at different temperatures.

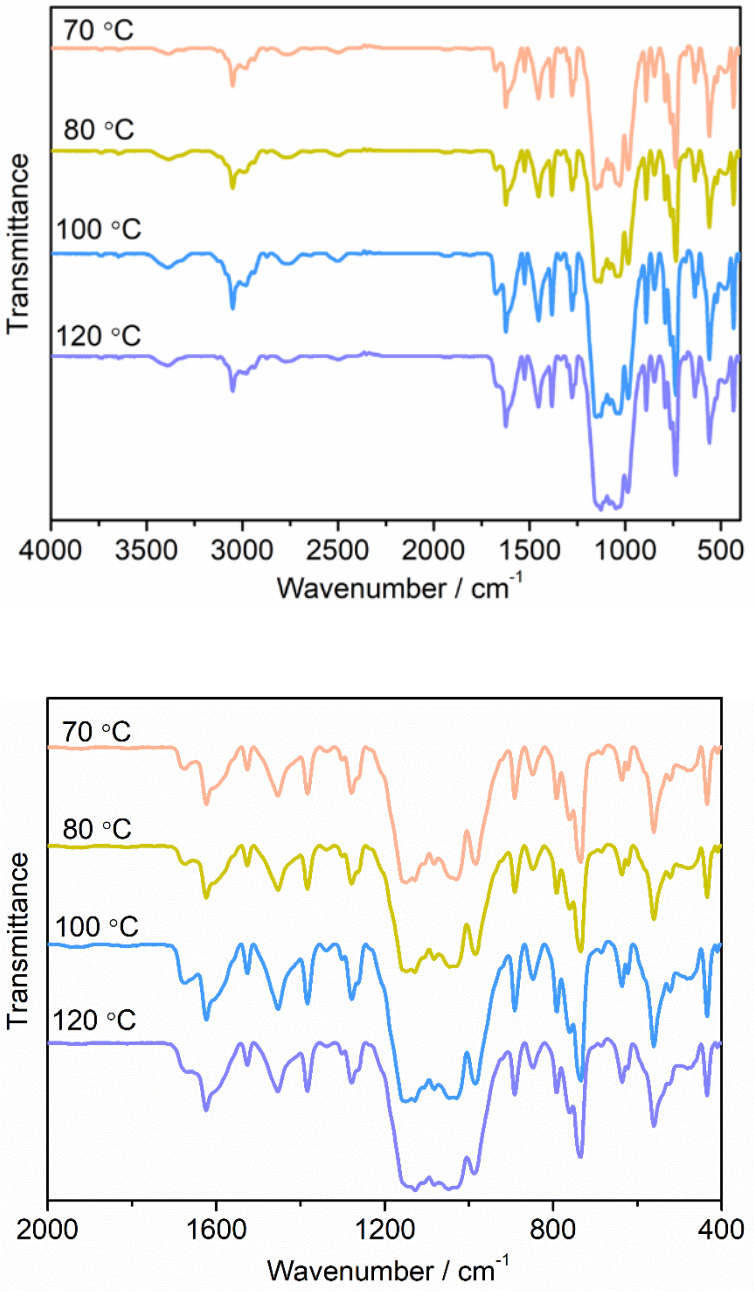

Figure S42. IR spectra of the $Gd(NO_3)_3$/*R*-AnempH_2 (1:3) assemblies obtained in 90 vol % NPA / DMF (total volume 5 mL) and 0.5 mL water at different temperatures, up 4000-400 cm^{-1}, bottom: 2000-400 cm^{-1}.

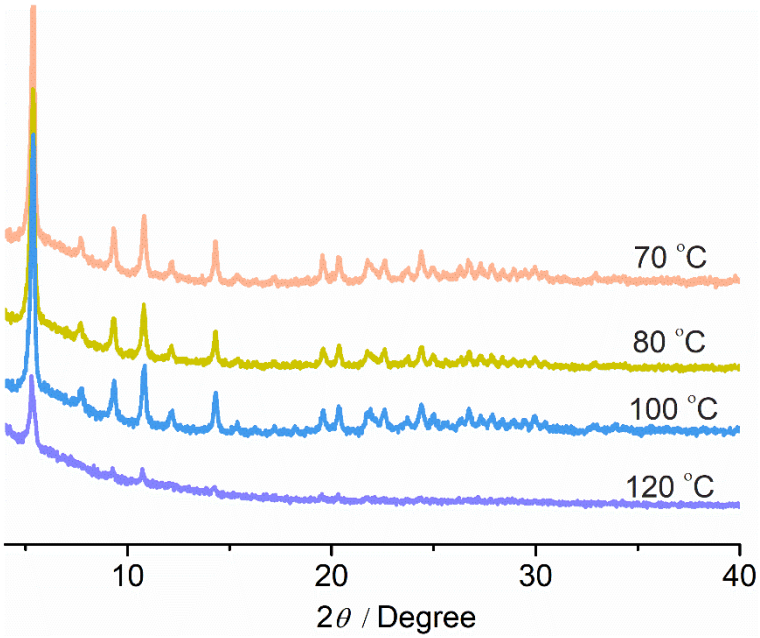

Figure S43. PXRD patterns of the $Gd(NO_3)_3$/*R*-AnempH_2 (1:3) assemblies obtained in 90 vol % NPA / DMF (total volume 5 mL) and 0.5 mL water at different temperatures.

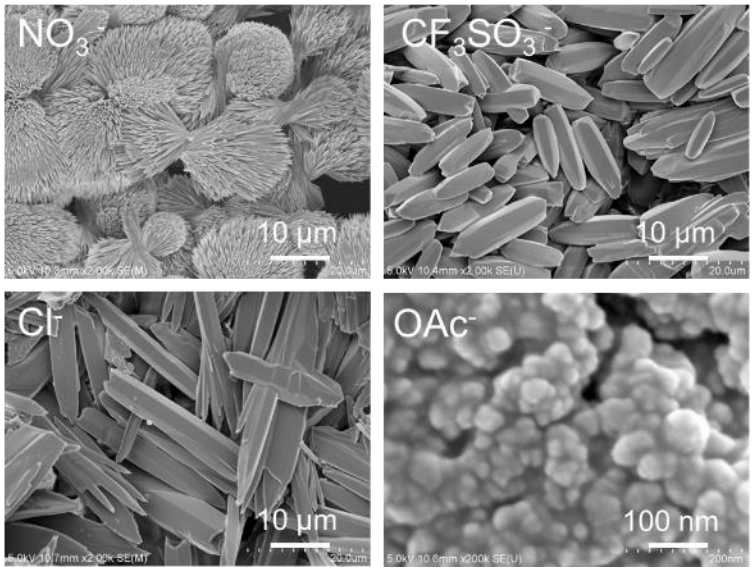

Figure S44. SEM images of the GdX_3/*R*-AnempH_2 (1:3) assemblies obtained in 90 vol % NPA / DMF (total volume 5 mL) and 0.5 mL water at 100 °C using different gadolinium salt [$Gd(NO_3)_3$, $GdCl_3$, $Gd(OAc)_3$ and $Gd(CF_3SO_3)_3$].

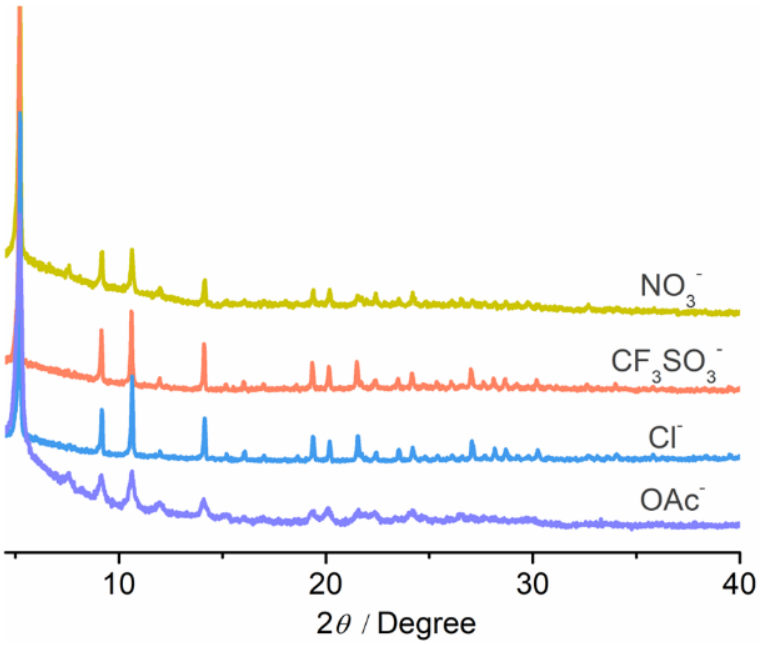

Figure S45. PXRD patterns of the GdX_3/*R*-AnempH_2 (1:3) assemblies obtained in 90 vol % NPA / DMF (total volume 5 mL) and 0.5 mL water at 100 °C using different gadolinium salt [$Gd(NO_3)_3$, $GdCl_3$, $Gd(OAc)_3$ and $Gd(CF_3SO_3)_3$].

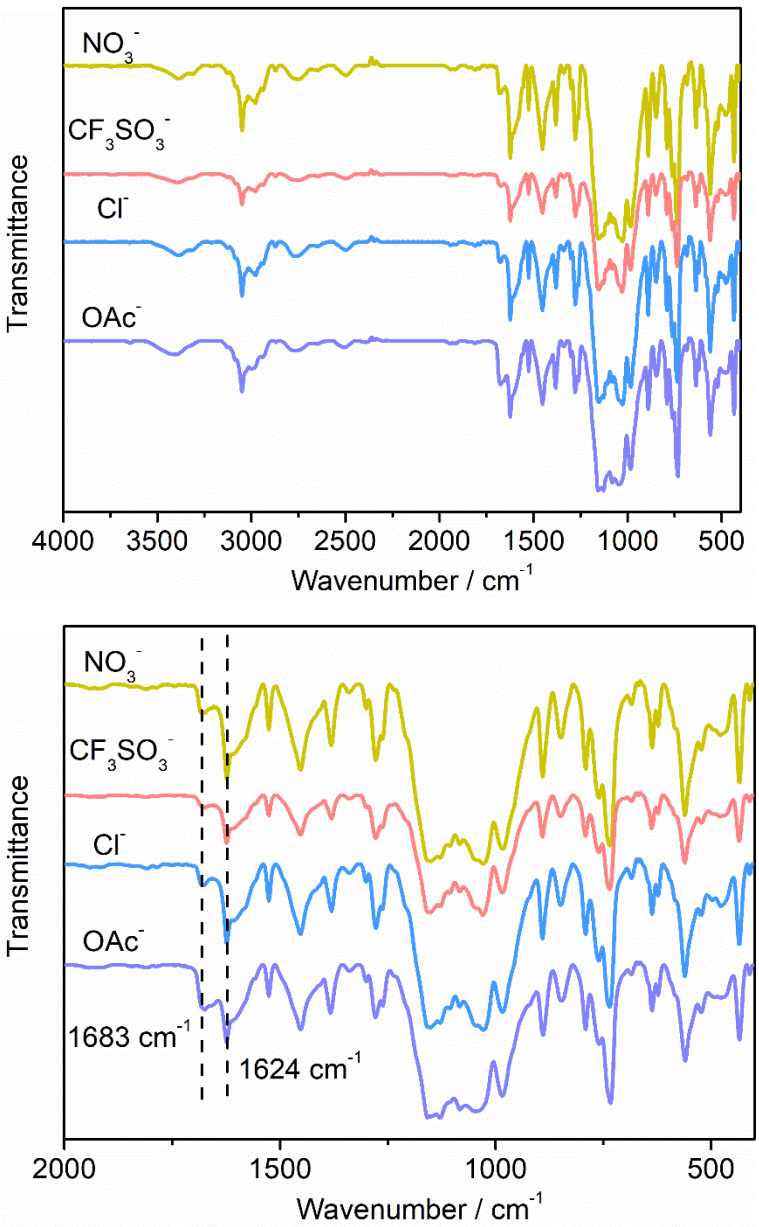

Figure S46. IR spectra of the GdX_3/*R*-AnempH_2 (1:3) assemblies obtained in 90 vol % NPA / DMF (total volume 5 mL) and 0.5 mL water at 100 °C using different gadolinium salt [$Gd(NO_3)_3$, $GdCl_3$, $Gd(OAc)_3$ and $Gd(CF_3SO_3)_3$], up 4000-400 cm^{-1}, bottom: 2000-400 cm^{-1}.

V. The influence of morphology on optical properties

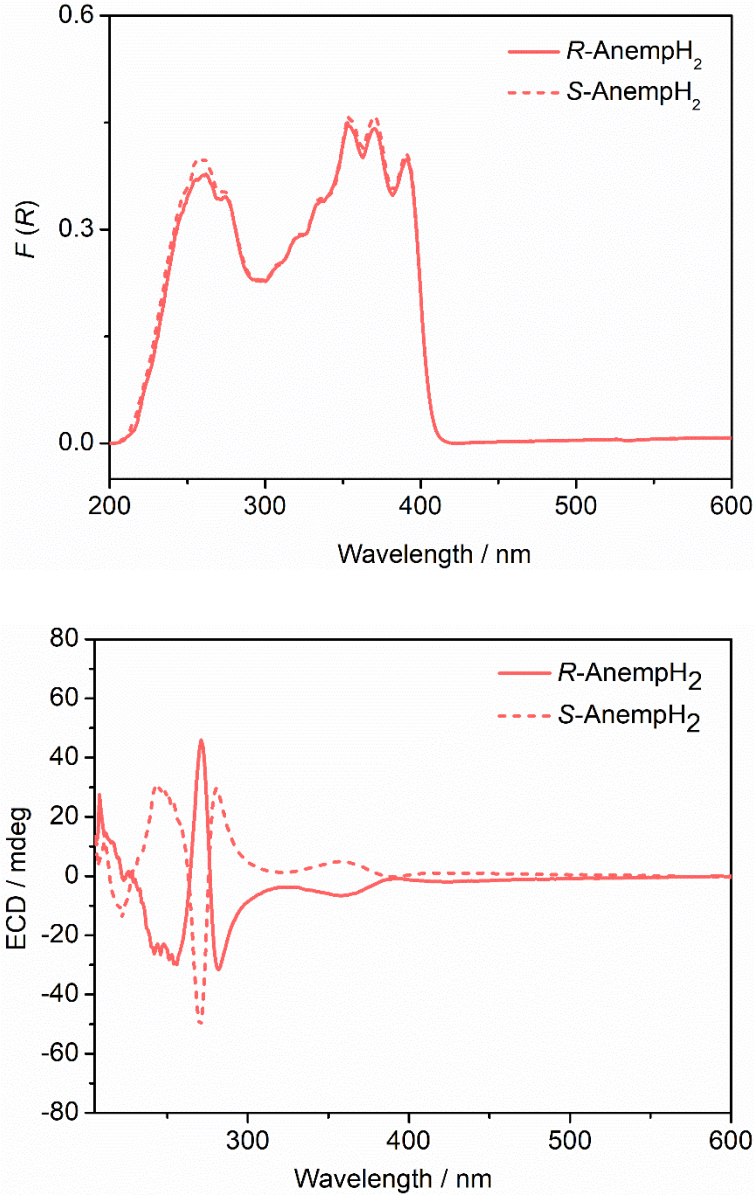

Figure S47. (top) UV-Vis spectra and (bottom) ECD spectra of *R*-, *S*-AnempH_2. The ECD measurements were performed on a JASCO J-810 spectrophotometer.

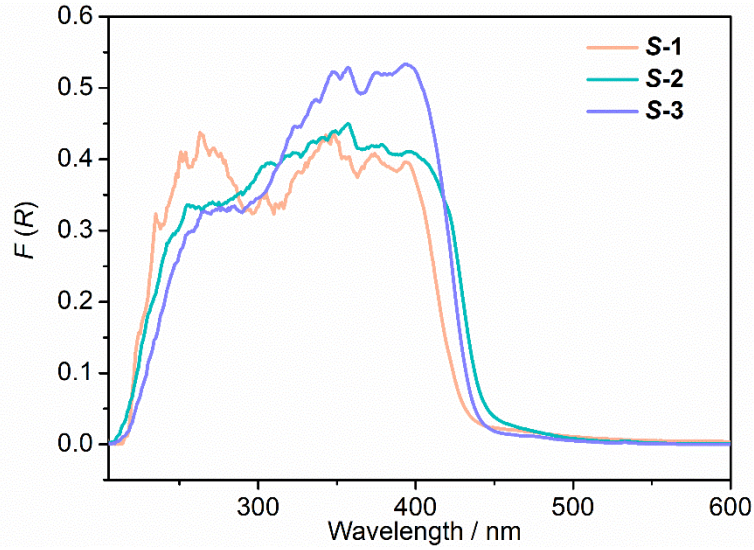

Figure S48. UV-Vis spectra of ***S*-1**, ***S*-2**, and ***S*-3**.

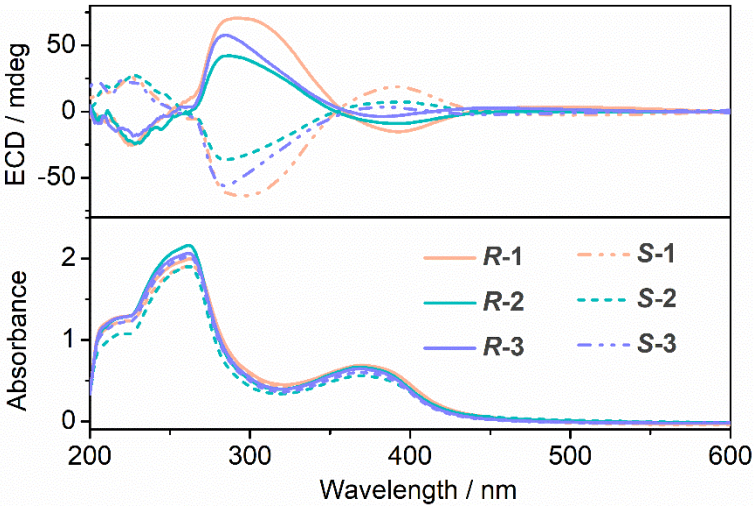

Figure S49. ECD spectra of ***R*-1**, ***S*-1**, ***R*-2**, ***S*-2**, ***R*-3**, ***S*-3**. The measurements were performed on a JASCO J-810 spectrophotometer.

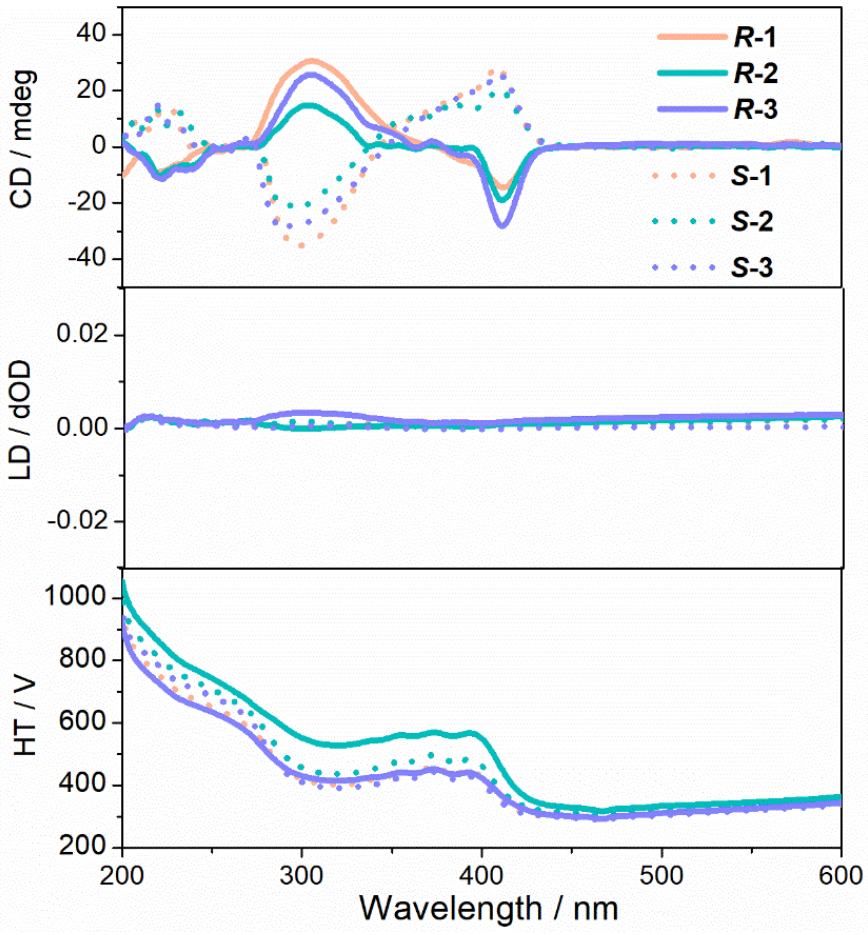

Figure S50. ECD spectra of ***R*-1**, ***S*-1**, ***R*-2**, ***S*-2**, ***R*-3**, ***S*-3**. The measurements were performed on a JASCO J-1700 CD spectrometer.

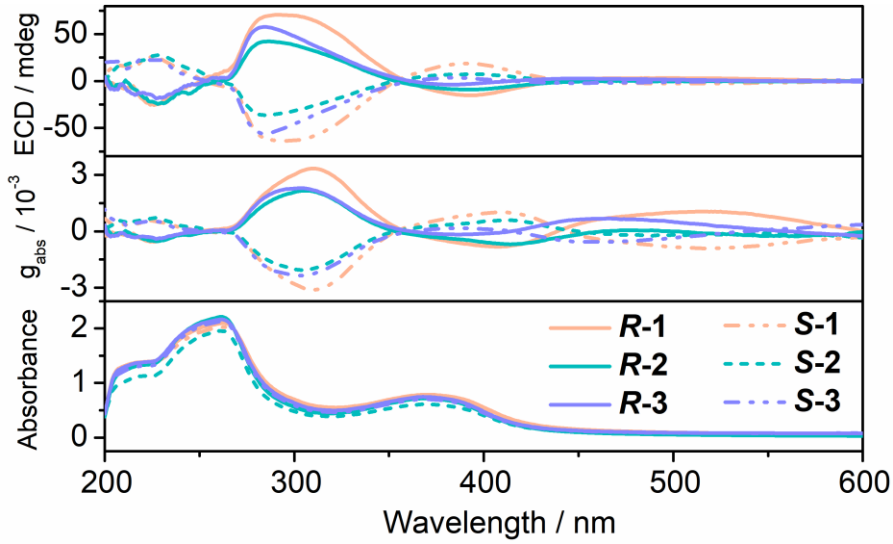

Figure S51. The ECD, g_{abs}, and absorption spectra of the R- and S-isomers of **1**, **2**, and **3**. The ECD measurements were performed on a JASCO J-810W spectrophotometer.

Table S7. The maximum emission peak, life time and quantum yield of ***R*-1**, ***S*-1**, ***R*-2**, ***S*-2**, ***R*-3**, ***S*-3**.

g_{abs}	***R*-1**	***S*-1**	***R*-2**	***S*-2**	***R*-3**	***S*-3**
225nm	-4.6×10^{-4}	5.1×10^{-4}	-4.5×10^{-4}	5.2×10^{-4}	-4.5×10^{-4}	5.0×10^{-4}
310nm	3.38×10^{-3}	-3.20×10^{-3}	2.18×10^{-3}	-2.05×10^{-3}	2.35×10^{-3}	-2.34×10^{-3}
425 nm	-9.6×10^{-4}	1.0×10^{-4}	-6.8×10^{-4}	6.3×10^{-4}	-1.8×10^{-4}	1.2×10^{-4}

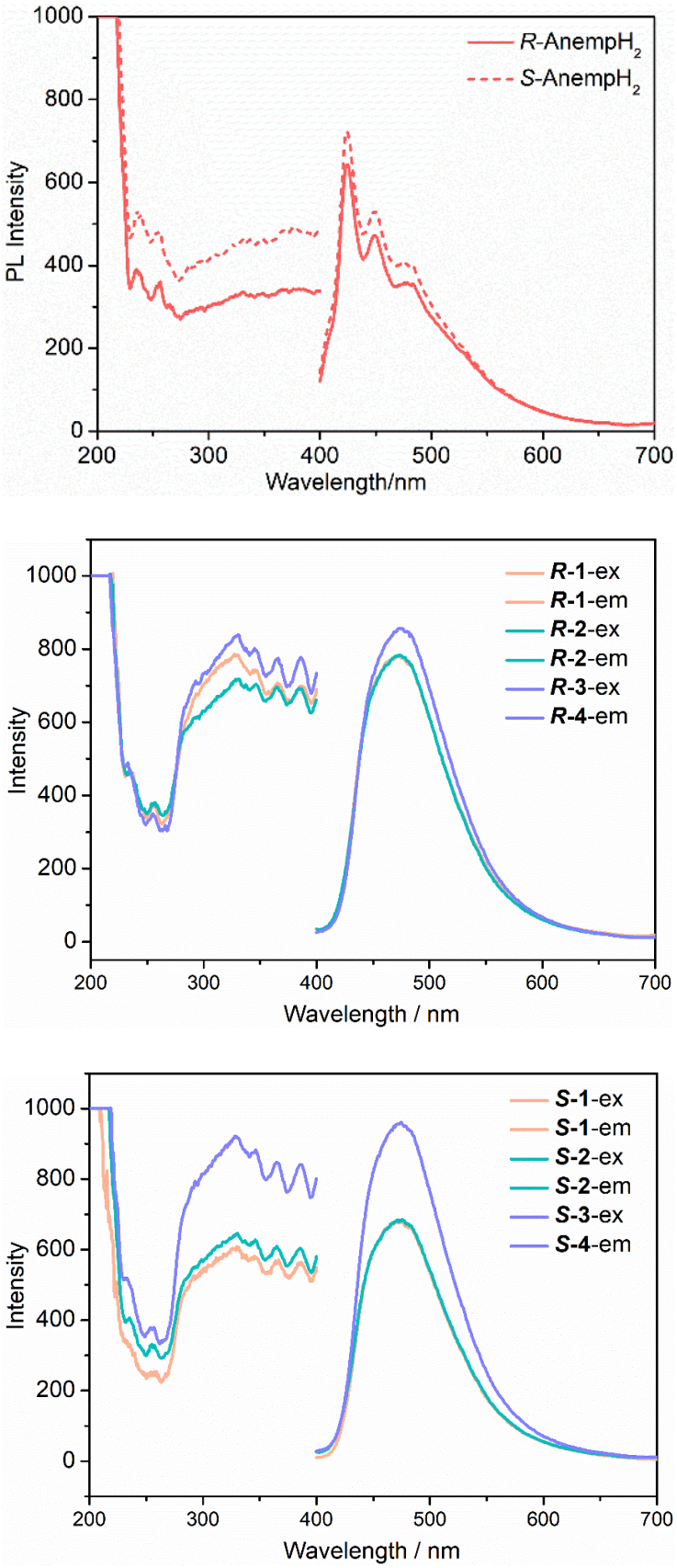

Figure S52. PL spectra of *R*- and *S*-isomers of ligand, **1**, **2** and **3**.

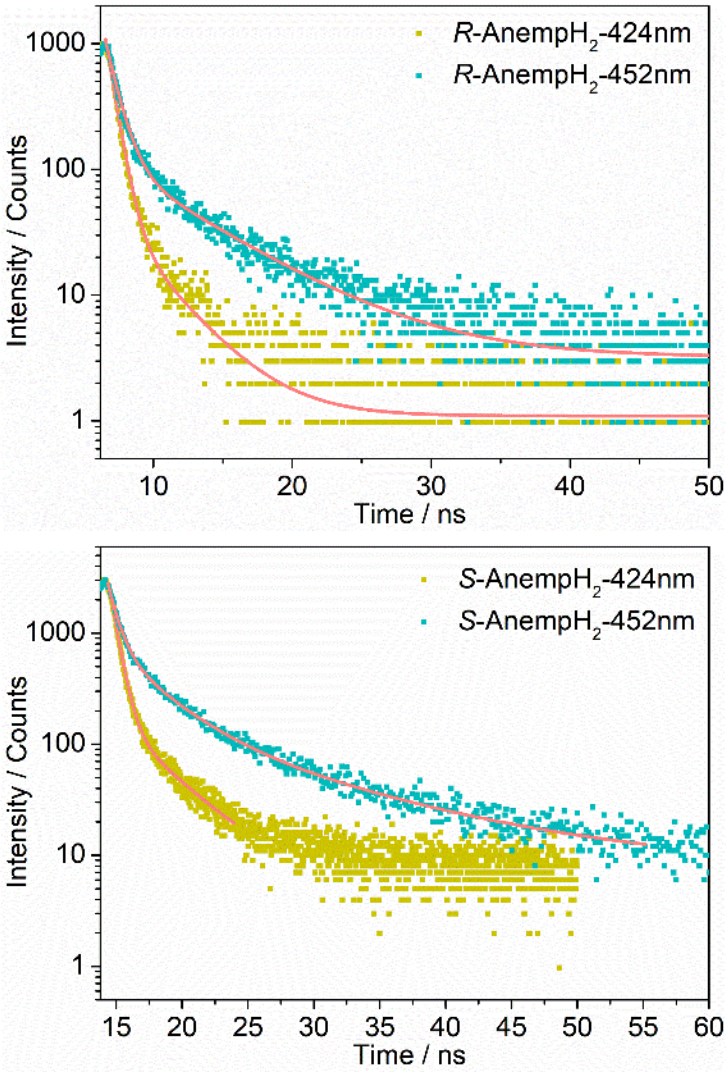

Figure S53. Fluorescence decay curves and fitting lines for *R*-AnempH$_2$ and *S*-AnempH$_2$.

Table S8. The maximum emission peak, life time and quantum yield of *R*-AnempH$_2$ and *S*-AnempH$_2$.

	R-AnempH$_2$-424nm	*R*-AnempH$_2$-452nm	*S*-AnempH$_2$-424nm	*S*-AnempH$_2$-452nm
λ_{em}	424 nm	452 nm	424 nm	452 nm
τ / ns	0.61(82.56%)	0.83(54.05%)	0.57(68.93%)	0.72(29.84%)
	3.24(17.44%)	6.21(45.95%)	3.92(31.07%)	3.38(37.84%)
				34.11(32.33%)
τ_{av} / ns	1.07	3.29	1.61	2.20
QY / %	1.28		1.11	

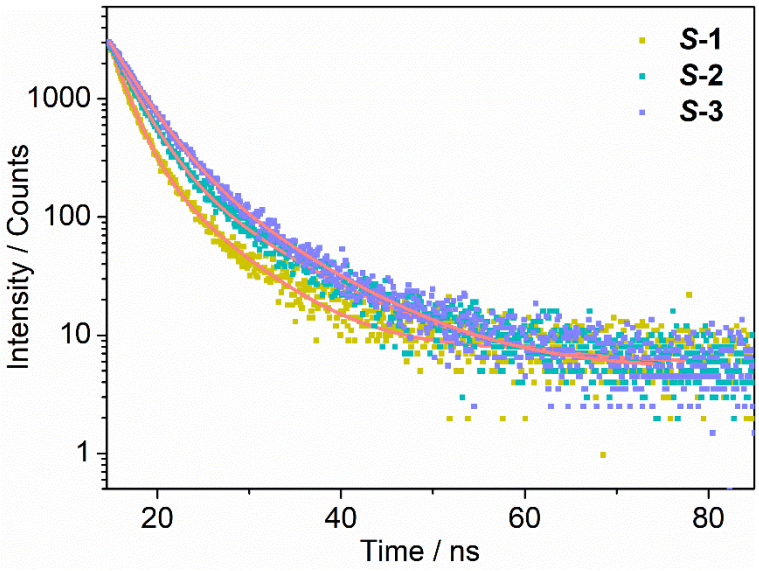

Figure S54. Fluorescence decay curves and fitting lines for ***S*-1**, ***S*-2**, and ***S*-3**, emitting at 484 nm.

Table S9. The maximum emission peak, life time and quantum yield of ***R*-1**, ***S*-1, *R*-2**, ***S*-2**, ***R*-3, *S*-3**.

	***R*-1**	***R*-2**	***R*-3**	***S*-1**	***S*-2**	***S*-3**
λ_{em}	484 nm	484 nm	484 nm	484 nm	484 nm	484 nm
τ / ns	1.81(67.73%)	3.00(69.53%)	3.77(74.02%)	1.81(66.53%)	2.63(69.27%)	3.14(67.16%)
	6.35(32.27%)	9.77(30.47%)	10.32(25.98%)	6.40(33.47%)	8.97(30.73%)	8.80(32.84%)
τ_{av} / ns	3.28	5.06	5.47	3.35	4.58	4.61
QY / %	0.88	1.30	2.41	1.12	1.23	1.96